MICROFABRICATION OF FLOW THROUGH CELLS WITH PARALLEL OPPOSED ELECTRODES FOR RECYCLING AMPEROMETRIC DETECTION

By

SUNDAY A. BROOKS

A DISSERTATION PRESENTED TO THE GRADUATE SCHOOL OF THE UNIVERSITY OF FLORIDA IN PARTIAL FULFILLMENT OF THE REQUIREMENTS FOR THE DEGREE OF DOCTOR OF PHILOSOPHY

UNIVERSITY OF FLORIDA

1997

Dedicated to the memory of my beloved mother, Nancy Ann Johnson Brooks

TABLE OF CONTENTS

Abstract of Dissertation Presented to the Graduate School of the University of Florida in Partial Fulfillment of the Requirements for the Degree of Doctor of Philosophy

MICROFABRICATION OF FLOW THROUGH CELLS WITH PARALLEL OPPOSED ELECTRODES FOR RECYCLING AMPEROMETRIC DETECTION

By

Sunday A. Brooks

August 1997

Chairman: Robert T. Kennedy
Major Department: Chemistry

Flow-through recycling electrochemical detectors with dual Au electrodes were fabricated using micromachining techniques. Detector cells contained two microband electrodes that were 50 μm wide by 3-5 mm long separated by a 5 or 10 μm gap in a parallel-opposed configuration. One electrode was defined in the bottom of a channel which was etched into the surface of a Si wafer while the other electrode was defined on a glass substrate. The depth of the channel defined the gap distance between the electrodes. The Si and glass pieces were anodically bonded together to create a flow cell. The stability and reproducibility of single and dual electrode cells were characterized with cyclic voltammetry and amperometry during flow injection analysis (FIA). Single electrode detectors had detection limits of 50 nM with root mean square noise in the 3-10 pA range. The dual electrode cells showed enhanced sensitivity over single electrode cells through detection of analyte molecules multiple times as they were transported through

the cell. Signal enhancements up to 60-fold were obtained with dual electrode cells during FIA at a flow rate of 50 nL/min.

Limitations encountered during characterization of parallel opposed detectors were addressed through several methods. A potentiostat headstage switching system was built to reduce noise increases encountered during dual electrode detection. By switching the working electrodes in and out of connection with the potentiostat, 1-5 nM LODs were achieved for ferrocyanide. Array electrodes were used in place of solid bands to reduce the area dependent noise contribution of single electrodes. A detection limit of 20 nM was achieved with an array of 10 μm wide fingers separated by 5 μm gaps. To obtain a detector with a wider potential window, carbon films were deposited and patterned to replace gold as the electrode material.

Random walk simulations were developed to model diffusional motion and detection of molecules in A) recycling electrochemical detectors, and B) detection of exocytosis products at a microelectrode. For recycling detectors the simulations were used to investigate recycling properties of possible detector designs and to predict signal enhancement during recycling detection. Random walks simulations were also used to predict current spike shapes obtained from detection of insulin and serotonin exocytosis. Simulated detection spikes were compared to experimental spikes to investigate differences in their method of transport to the electrode.

CHAPTER 1
INTRODUCTION

The use of microscale separation techniques in biological and pharmaceutical analyses has expanded its scope in recent years. The growing number of microscale analyses have prompted investigation of more sensitive photospectrometric and electrochemical detection (ECD) methods for these techniques. In this work microfabrication technology was used to develop flow through electrochemical cells compatible with microcolumn separation systems which are capable of improving sensitivity by electrochemical recycling of reversible analytes.

Electrochemical Detection in Flowing Systems

Electrochemical detection in flowing streams is used in many analytical techniques such as flow injection analysis (FIA), continuous flow sensors, chromatography, and capillary electrophoresis (CE). Three basic modes of electrochemical detection have been utilized in flowing streams (1). Conductometric techniques measure conductance, while potentiometric techniques monitor potential changes between two electrodes when an electroactive compound is introduced or removed from the solution. The third mode, amperometry, is the measurement of current which results when compounds in solution lose or gain electrons at the electrode surface. The current measured is proportional to the concentration of analyte present. Coulometric detection is a specific type of amperometry where 100 % of the analyte is oxidized or reduced.

Direct current amperometry, where current is measured at a fixed applied potential, is the most commonly used finite-current electrochemical technique (2). Its usefulness stems from a combination of sensitivity, selectivity, and versatility (1,3). Amperometry can be more sensitive than other modes of ECD due to the lower background levels and lower noise resulting from the fixed potential compared to scanning, which introduces double layer charging currents. Selectivity and versatility result from being able to choose a specific potential for detection of an analyte, therefore eliminating or reducing interferences from other compounds present in a sample.

There are several advantages to using ECD over other methods. Low limits of detection, in the nanomolar range, are possible without derivatization for some analytes. Low detection limits are possible because ECD directly converts chemical information into electrical signal by the loss or gain of electrons from the analyte of interest. Also, ECD is inherently selective; it can be used to differentiate between compounds based on their redox potentials, or the specific potentials necessary to induce electron transfer. Oxidation states of elements can also be differentiated based on their specific redox potentials. Other advantages of ECD are its low cost compared to techniques such as spectroscopy and also relatively easy miniaturization of electrodes.

Electrochemical Detection in Liquid Chromatography

The electrochemical detector for LC was developed in Ralph Adams' laboratory at the University of Kansas in the early 1970s (3). High performance liquid chromatography with electrochemical detection (HPLC-ECD) first became popular for its applicability to the study of aromatic amines and phenols in the central nervous system, and most papers

published during its history have focused on neurochemical problems (2). Since then ECD has been widely applied with LC to the trace determination of easily reduced or oxidized organic compounds. LC requires a selective detector with a rapid response time, wide dynamic range, and low dead volume. ECDs that fit this description are fairly simple to build and to interface to separation columns. After the first commercial detectors became available in 1974, the areas of application of this technique have expanded to include sulfur, nitroso, nitro compounds, and organometallics (2,4).

The material used as an electrode in an LC-ECD experiment must be sturdy and have long term stability. Different forms of carbon are widely used including glassy, vitreous, pyrolytic, graphite paste, and fiber. Carbon is relatively inexpensive and has a wide useful potential range. Mercury has been used in flow cells as amalgamated gold disks. Dropping mercury electrodes have also been used as LC detectors, but due to the difficulties of coupling drop electrodes with LC, high double-layer charging, and clogging, they are not competitive with stationary electrodes (5). Noble metal electrodes such as gold (Au) and platinum (Pt) are used to detect compounds which are not detectable at carbon fibers. Alcohols, glycols, carbohydrates, sulfur compounds, amines, and amino acids can interact with empty d-orbitals on the surface of a metal electrode to form electroactive species (1). However, this surface characteristic can also result in fouling of the electrode surface. Both carbon and metal electrodes can be chemically modified to improve and expand their applicability.

Column diameters in HPLC are usually in the millimeter (mm) range, with electrodes of mm dimensions. Several configurations of ECD cells are used in practice

with HPLC. Tubular electrode configurations, where solution flows through a tube made of electrode material, have been used. This configuration is usually limited to metal electrodes due to the cylindrical design. Packed bed electrodes, which can be tubular or planar, can be used to increase conversion efficiency (Figure 1-1). The cell configuration most used in LC is a cross-flow thin layer cell as shown in Figure 1-2. The volume of this type of electrochemical cell ranges from one to a few microliters, with flow rates through the column and detector in the μL/min range. The flow rates and volumes used result in low conversion efficiencies of the analyte, usually a few percent. Concentration detection limits are in the low nanomolar range, with mass detection limits from femto- to picomoles for thin layer cells.

ECD in LC is not limited to a single working electrode, and dual and multielectrode detectors of several geometries have been constructed (6). Configurations of several dual electrode detectors are shown in Figure 1-3. The dual-parallel adjacent configuration is used to monitor current at two different potentials (Figure 1-3 A). With single electrode detection, the potential must be sufficient to oxidize (or reduce) all of the compounds of interest. The complexity of the chromatogram at a higher detection potential can obscure the response of more easily oxidized (reduced) analytes. With the dual-parallel electrode configuration, high and low detector potential chromatograms can be obtained simultaneously. Therefore, this arrangement can be used to quantitate an easily oxidized (or reduced) substance in the presence of others which react at higher potentials. With the dual-series configuration, the products of the upstream electrode are monitored at the downstream electrode (Figure 1-3 B). Using a second electrode

upstream can enhance selectivity by either modifying analyte components so that a more informative chromatogram is obtained at the downstream electrode, or by removing interfering compounds before they reach the downstream electrode.

The goal of the work described in this dissertation was to increase the sensitivity of the electrochemical detector; therefore, the parallel opposed detector was well suited to this purpose. Through electrochemical recycling, this detector can improve sensitivity and detection limits by enhancing the signal measured per molecule (7). As shown in Figure 1-3 C, two working electrodes are positioned parallel to each other across a flow channel. One electrode is fixed at a potential sufficient to oxidize the analyte and the other fixed at a potential sufficient to reduce the oxidized product back to its original state. If the electrodes are spaced closely, individual analyte molecules can be electrochemically recycled by diffusing back and forth between the electrodes as they flow through the cell resulting in detection of individual molecules multiple times, resulting in enhanced signals, as illustrated in Figure 1-4. The amount of recycling observed is dependent on the time required for molecules to diffuse from one electrode to the other and the residence time of analyte in the detector (8). This approach can also enhance selectivity as only reversible compounds are recycled (7,8). This was the ECD of choice for most of this work, and will be discussed in more detail in Chapter 2.

A second detector capable of electrochemical recycling is the interdigitated array (IDA) as shown in Figure 1-3 D. Two array electrodes are positioned such that the fingers of one array alternate with the second on the flow cell surface. The two arrays can be biased at reduction and oxidation potentials of analytes as described above. As the

analyte flows through the detector cell, each molecule can be recycled as it travels between the oppositely charged fingers of each array. The theoretical aspects of this generation/collection process have been investigated by Ou, Moldoveanu, and Anderson (9). Microfabrication of this detector was also investigated in this work.

The availability of commercial ECDs for HPLC both with single and dual electrodes has resulted in the development of detection methods for most classes of compounds. Most applications are designed for pharmaceutical, environmental, neurochemical, or other biological analyses. For example, phenolic compounds of biological interest such as catecholamines and plant phenolics and also of industrial interest have been detected via oxidation at graphite electrodes (10,11). Thiols have been oxidized to disulfides at mercury and Au electrodes (12). Other compounds analyzed by oxidation in HPLC-ECD include ascorbic acid, uric acid, and NADH. Reductive detection of quinones in HPLC-ECD has been used for a large number of natural and synthetic product analyses. Nitro and nitroso compounds have been reduced at both mercury and carbon electrodes. Many pharmaceuticals, explosives, and agricultural chemicals are in this group and several HPLC-ECD methods have been developed to analyze them (10,13,14). Organometallics can also be analyzed with reductive HPLC-ECD (15).

In addition to direct oxidation or reduction, pre- or post-column derivatization can be used to expand the application of HPLC-ECD. Orthophthalaldehye (OPA) has been employed as a precolumn tagging reagent for detection of primary amine analytes (16,17). An example of a post-column reaction is the detection of peptides using the biuret reaction

(18). Peptides react with Cu(II) to form complexes, which can then be detected by the oxidation of Cu(II) to Cu(III).

Microcolumn LC-ECD Systems

One approach which has improved detection limits in LC-ECD is miniaturization. A representative microcolumn LC-ECD system is shown in Figure 1-5. Microcolumn separations typically have columns of 10-100 μm inner diameter and electrodes (carbon fiber) of micrometer diameters or dimensions. Miniaturization has made possible analysis of very small volumes (nanoliters) of sample, which allows sampling of very small environments difficult to analyze with conventional separations instrumentation. The first on-column ECD for microcolumn LC was a 1 μm diameter ion selective electrode which was used to detect potassium ions in open tubular liquid chromatography (OTLC) with detection limits in the picomole range (19). The first example of microcolumn LC-ECD amperometry used a 9 μm carbon fiber in the end of a 15 μm i.d. OTLC column to achieve femtomole detection limits for ascorbic acid, catechol, and 4-methylcatechol (20).

Microelectrodes have concentration detection limits similar to conventional electrodes (i.e. low nanomolar), but when paired with microcolumn separations, they allow mass detection limits in the low attomole range; this is ~1,000-fold lower than conventional HPLC electrochemical detectors (21,22). This improvement in detection results from the high efficiency of the microelectrode, which is placed directly in the end of the separation column, achieving 80-90% conversion of the analyte (Figure 1-5). Lower background levels and lower ohmic drop of microelectrodes compared to regular size electrodes also contribute to the improved performance of microcolumn LC-ECD.

However, there is little commercial instrumentation available, such as injection valves, for microcolumn LC-ECD. Detection in microcolumn LC-ECD has been mostly limited to carbon fibers; investigation of other types of ECDs could further improve detection limits.

Applications of microcolumn LC-ECD have been developed for analysis and separation of single-cell components (1). Neurotransmitter and amino acid levels were determined by fast-scan voltammetry in the whole-cell analysis of neurons from the snail *Helix aspersa* (23). Non-electroactive amino acids from the same type of invertebrate were derivatized with napthalene-2,3-dicarboxaldehyde (NDA) and determined amperometrically (24). Norepinephrine and epinephrine were amperometrically measured from single bovine adrenomedullary cells (22).

Microfabrication Technology

The decrease in sample volume with microcolumn separations compared to HPLC, and therefore the amount of sample available for analysis, has prompted investigation into miniaturized and more sensitive detection methods for these techniques. Microfabrication technology is primarily used in the production of miniaturized integrated circuits, allowing mass batch-fabrication of hundreds or even thousands of circuit chips on a single wafer (25). Microfabrication processes are extremely reproducible at the wafer scale for patterning metals, semiconductors, and dielectrics. The definition and reproduction of film patterns and structures using photographic techniques can be done with high precision at the micron and submicron levels. Procedures for creating these layers can be summarized in three steps: deposition of metal or dielectric material, application and patterning of a mask layer, and the etching or removal of the layer exposed through the mask.

Photolithographic (often called microlithographic) patterning is used to define spatially where deposition or etching occur on the substrate surface. Photoresists, or photosensitive polymers, are spin coated onto the wafer or layer to be patterned, then "soft-baked" to drive off solvents. Soft-baked refers to a temperature which only evaporates solvents and is below the temperature which initiates cross linking reactions. The layer is then exposed to UV light through a photomask, which is usually a metal pattern on a glass plate, and exposed photoresist is either removed (called a positive reist) or is crosslinked (negative resist) upon development.

Since the fabrication of the computer chip, this technology has also been applied to making mechanical structures in addition to electronic ones. Cantilever beams, thin beams of silicon dioxide supported at only one end, were suspended over a shallow pit in silicon (26). These beams were used for applications such as miniature accelerometers invented for use in-vivo to measure heart accelerations (27). Ink jet nozzles have been fabricated by directional etching through silicon wafers (28). A micromirror projection display was described which consists of an array of up to 4 million moveable mirrors that can be individually tilted on or off by applying a voltage (29). When activated, the mirrors can project color video images onto a screen. Other mechanical devices which have been developed include pressure sensors.

More recently, these techniques have been applied to chemical instrumentation. The most significant early report of a chemistry related device was the gas chromatograph on a wafer built at Stanford in 1979 (30). The importance of this device was that the entire system was contained on the silicon chip: a separation column, an injector, and also

a thermal nickel detector. Although a quite complex design, it was used only to detect a mixture of simple gases.

Several groups have investigated CE systems fabricated on glass microchips with spectroscopic detection (31-36). An immunoassay has been performed on a microchip electrophoretic system which can determine serum cortisol in blood serum over the range of clinical interest (31). Sequencing of DNA and polymerase chain reactions have been initially investigated with these devices (32,33). A unique type of separation channel, a cyclic planar structure which is the intersection of four single channels, has been used to perform an MECC-based immunoassay for serum theophylline (34).

Microfabrication has also been used to develop electrodes and ECDs. Disk, band, and array electrodes have been constructed with gold, platinum, metal oxides, and carbon electrode materials. Voltammetric studies in static solution have been done with a three electrode cell-on-a-chip, microfabricated arrays, and IDAs (37,38). IDAs have been used both for fundamental studies, such as measurement of diffusion coefficients through polyacrylate gels, and for analysis, such as measurement of 4-aminophenol by immunoassay and of glucose with an imaging array detector (39,40,41). Also, an on-line sensor was developed to monitor changes in extracellular L-glutamate concentration as a result of stimulated release from nerve cells with a detection limit of 7.2 nM (42).

In addition, microfabricated band and array electrodes have been investigated recently as CE detectors (43-45). An initial study characterized a conductivity detector with Pt band electrodes which measured Li^+ and K^+ ions at a concentration limit of 0.7 μM (43). A Pt microband array electrode on a silicon chip was confined to a flow channel and connected to a CE capillary as a detector (44). It was capable of detecting

1.4 fmol of hydroquinone but with reduced efficiency compared to regular on-column CE detection. Another CE detector recently developed had 100 gold microelectrodes positioned at the exit of a wide flow channel. The end of a CE capillary was moved across the channel, allowing continuous separations (45). Even with these advances, the area of microfabricated electrochemical detectors for microcolumn separation techniques is still at the early stages of development, and is a relatively unexplored area for investigation.

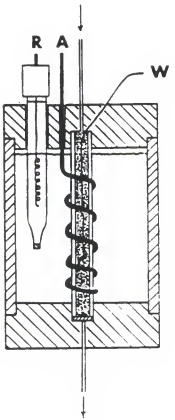

Source: (2) Lunte, S.M., Lunte, C.E., and Kissinger, P.T. in *Laboratory Techniques in Analytical Chemistry*, 2nd ed. Marcel Dekker, Inc., 1996.

Figure 1-1. Flow-through packed bed coulometric reactor. The working electrode is labeled W, the auxiliary electrode is labeled A, and the reference electrode is labeled R.

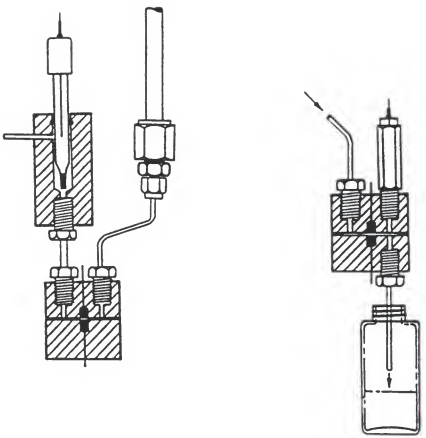

Source: (2) Lunte, S.M., Lunte, C.E., and Kissinger, P.T. in *Laboratory Techniques in Analytical Chemistry*, 2nd ed. Marcel Dekker, Inc., 1996.

Figure 1-2. Commercially available thin layer LC/ECD detectors.

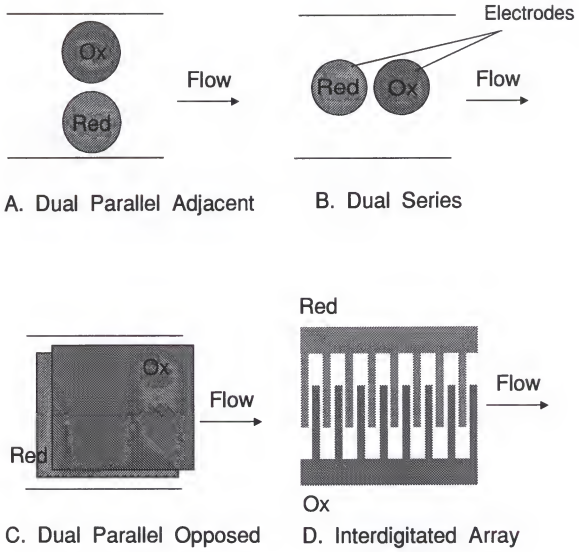

Figure 1-3. Top view of dual electrode geometries. The types shown are limited to those used in LC.

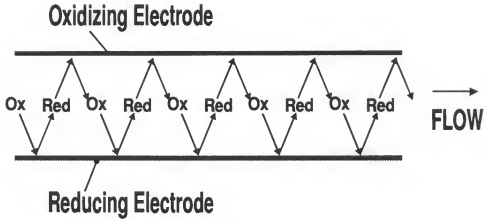

Figure 1-4. Recycling electrochemical detection with parallel opposed geometry. Analyte molecules diffuse between the two electrodes as they travel through the flow cell, resulting in their detection multiple times.

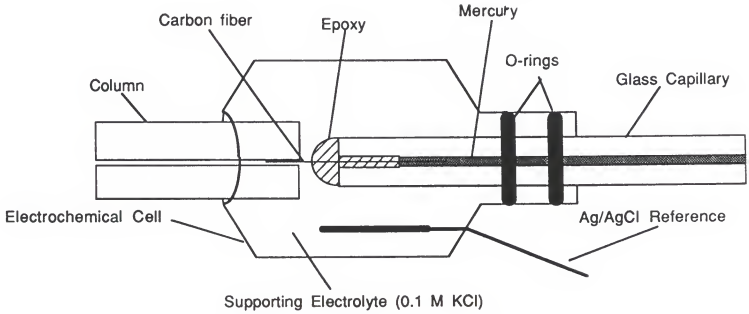

Source: Kennedy, R.T. Ph.D. Dissertation, University of North Carolina Chapel Hill, 1988.

Figure 1-5. Microcolumn LC/ECD experimental configuration. The tip of the carbon fiber is inserted directly into the end of the separation capillary. Connection is made by immersing the detector in a buffer reservoir where

CHAPTER 2
PARALLEL OPPOSED RECYCLING ELECTROCHEMICAL DETECTORS

Introduction

The goal of this project was to fabricate electrochemical detectors that would improve the sensitivity of microcolumn separation methods. As described in the previous chapter, miniaturization was one method successfully used to improve mass detection limits in chromatography. Other routes to improving sensitivity and detection limits are enhancing the signal measured per molecule without increasing the noise level present, or reducing the noise level itself. Recycling amperometric electrochemical detection was the method of choice for this work. As described in Chapter 1, electrochemical recycling occurs when two working electrodes are biased at the reduction and oxidation potentials of the analyte of interest. Molecules can then be detected multiple times as they pass through the flow cell and diffuse between the two electrodes as shown in Figure 1-4.

Recycling electrochemical detection, also called regenerative electrochemical detection, has been investigated in flowing streams with several electrode geometries (7,8,47-50). For example, Matsue, Aoki, Abe, and Uchida used IDAs with a total electrode area of 0.02 cm^2 and flow rate of 1 mL/min to enhance the response of catecholamines in the presence of ascorbic acid (47). Most flow studies of electrochemical recycling have utilized the parallel-opposed geometry shown in Figures 1-3 and 1-4 with macroelectrodes (areas ~0.2 cm^2) separated by Teflon spacers 20-100 μm

thick and flow rates compatible with HPLC, i.e. 10 to 1000 μL/min (7, 8, 48-50). Under these conditions, residence times of analyte in the detector cell are short and signal enhancements over single electrode cells are 5-10 fold (48, 49).

In an investigation of the parallel-opposed geometry, Purdy and Weber predicted that recycling electrochemical detection would be most beneficial when used with microcolumn separations where flow rates are in the nL/min range (8). At low flow rates, the residence time of analytes for a given electrode separation should be relatively long, even with closely spaced electrodes, allowing better recycling. Improved recycling combined with the enhancements in mass detection limit expected with microelectrodes could result in detection limits better than the low attomole (low nanomolar concentration detection limit) presently possible by amperometry. One difficulty with implementing the idea of recycling electrochemical detection compatible with microcolumn separations and low flow rates is fabrication of electrochemical cells. The total volume of the cell must be in the nanoliter range and electrode gaps must be on the order of micrometers for the electrodes to be analytically useful.

Microfabrication, with the advantages of precision and reproducibility, was the route chosen in this work to prepare electrochemical cells with the desired geometry and dimensions. Flow-through recycling electrochemical detectors with dual parallel Au electrodes were fabricated using this technology. Au was the chosen electrode material because it had well established deposition and etch processes. Detector cells contained two microband electrodes that were 50 μm wide by 3-5 mm long separated by a 5 or 10 μm gap in a parallel-opposed configuration. One electrode was defined in the bottom of a

channel which was etched into the surface of a Si wafer while the other electrode was defined on a glass substrate. The depth of the channel defined the gap distance between the electrodes. The Si and glass pieces were anodically bonded together to create a flow cell. The stability and reproducibility of single and dual electrode cells were characterized with cyclic voltammetry and amperometry during FIA .

Experimental

General fabrication. The construction of electrochemical flow cells was done at the microelectronics laboratory at the University of Florida, in a Class 100 clean room environment. The flow-through parallel opposed electrochemical detector cells were constructed in two pieces which were then anodically bonded together to form the detector cell as depicted in Figure 2-1. One piece consisted of a Si wafer insulated with silicon dioxide (SiO_2) which had a channel etched into the surface and a Au microband electrode defined on the bottom of the channel. The second piece consisted of flat Pyrex (Corning #7740) with a Au microband electrode defined on the surface. Each piece had a hole drilled or etched completely through which was used as a port for flow.

The first step to creating a channel or electrode is to create the desired pattern for photolithographic masking. The detector described in this chapter required three masks: one to define the pattern of the flow channels, a second to define the outlet/inlet holes, and a third to define the electrode position. This was done using the Magic software provided by the microelectronics lab; this program is designed for creating integrated circuit layouts and patterns. Simple commands were used to define the light (light will pass through) and

dark (light will not pass through) portions of the mask. Once finished, the mask pattern was copied and a mask fabricated by the staff at the microelectronics laboratory.

Etching of flow channels and outlet/inlet holes. The steps used to prepare the flow channel in the silicon wafer are shown in Figure 2-2. The importance of the cleaning procedures used in this work cannot be stressed enough. Silicon wafers 2 inches in diameter were "piranha etch" cleaned before use. A beaker of sulfuric acid was heated to a temperature of 120 degrees Celsius (°C). The beaker was then removed from heat and approximately 20 milliliters (mL) of 30% hydrogen peroxide was added; the amount varied and should be just enough to cause bubbling of the acid. A Teflon slotted holder housing the silicon wafers was immersed in the solution, and the beaker returned to heat. The temperature was maintained at 120 °C for 10 minutes. After removal from the acid, the wafers and holder are rinsed in deionized (DI) water for 5 minutes. The wafers were surface dried with pressurized nitrogen gas. Failure to properly clean the surfaces of the samples at all steps of fabrication resulted in dust or residue contamination. Effects of contamination include lack of adhesion of photoresist or metals and irregular etching results, which can cause total failure of the samples.

After cleaning, the wafers were oxidized in a quartz tube furnace at 1050 °C for 30 minutes to produce a 0.4 micron thick layer of SiO_2. The oxide layer was grown by introducing oxygen gas into the furnace tube during heating. An approximate growth chart for the oxide was provided by the laboratory, as was a table which related wafer surface color to amount of oxide present. These were used to approximate the thickness of oxide present for most experiments. Alternatively, an ellipsometer was available for use

in the microelectronics lab, which could measure the exact thickness. The thickness of the first oxide layer was not critical; it was only used as a mask for a brief time.

To prime the wafers for photoresist application, 20-30 mL of hexamethyldisilazane (HMDS) was placed in a box (in the fume hood) with one end raised to keep the fluid at the lower end. The wafers and holder were placed in the box at the raised end and the box covered. The wafers were vapor primed in this manner for 5 minutes.

Hoechst-Celanese positive photoresist (AZ 1370) was spin coated onto the wafers for 30 seconds at 4000 rpm, resulting in a film approximately 1.5 μm thick. This resist was replaced later by the company with AZ 1512. The information sheet describing this resist provided a spin speed vs. photoresist thickness curve to estimate photoresist thickness. The wafers were soft-baked at 90 °C for 30 minutes, as specified by Hoeschst-Celanese to drive off solvents. Thickness of the resist layer applied can be optimized for precise pattern definition.

The resist film was exposed to ultraviolet (UV) light through a chrome-on-glass mask using a contact mask aligner. The mask aligner consists of a mercury source lamp and aligning microscope. The sample was aligned at the desired position underneath the mask using an X-Y-θ stage, and the wafer brought in contact with the mask. Exposure time for this step (with AZ 1370 or 1512) was 18 seconds. The exposure time must be optimized for each photoresist type and thickness. If exposure time was too short, photoresist residue that should have been removed was seen under microscopic examination after development. If the exposure time was too long, extra photoresist was

removed, resulting in lower resolution of the pattern. This could be observed as rounded corners for large structures (>25 μm) or the absence or combining of small structures. For example, if two separate exposed lines separated by a 3 micron wide line of photoresist were joined, it was due to loss of photoresist between the lines from overexposure.

The wafer was developed by dipping in a commercial developer Hoechst-Celanese 312 for 30-60 seconds and rinsing with deionized water; over- and under-development had similar effects as described for exposure. A hard-bake step at 120 °C usually followed development to cross link the photoresist, making it impervious to etching procedures. However, hard-baking was unneccessary for this particular step; the etching of silicon oxide which followed was of short duration and did not damage the photoresist.

Exposure and subsequent development defined the flow channel pattern, leaving a photoresist mask for etching of exposed oxide with BOE. Oxide removal was complete was when water beaded on the surface of exposed areas instead of wetting them, indicating a hydrophobic silicon surface. Photoresist was removed with acetone, leaving an oxide mask and exposed Si pattern, and the wafers were rinsed in DI water. Channels were etched isotropically into wafer surfaces using a 50/20/1 (by volume) mixture of concentrated HNO_3, H_2O, and HF which etched at a rate of approximately 0.5 μm per minute. The depths of channels (5 or 10 μm) were monitored during etching using a Dektak IIA profilimeter. After the channels were etched, oxide mask was removed with BOE and rinsed. Wafers were divided into individual samples using a diamond tipped scribe, and again piranha etch cleaned.

To create outlet and inlet holes through wafers, a similar procedure to that described above was used. After flow channels were etched and the samples cleaned, a new layer of oxide was grown for a duration of 1.25 hours, resulting in an oxide layer of approximately 1.5 μm thick. This was necessary to create a mask thick enough for the long second etch step. A second, thicker layer of photoresist (AZ 1375) was applied and soft-baked at the same time and temperature as described above (~3 μm thick). A thicker layer of resist was applied to protect etched flow channels. Too thin of a layer of resist resulted in breakage of the layer on the corners of the flow channel, which resulted in unwanted etching of this area. The AZ 1375 resist was later replaced with AZ 1529. The samples were exposed through a second mask which defined square inlet (0.5 mm x 0.5 mm) or outlet (3 mm x 3 mm) holes in the photoresist. Exposure time for this step was 45 sec. After developing, a hard-baking step was once again not necessary. Exposed oxide was etched with BOE as previously described, and photoresist was removed with acetone, leaving an oxide mask.

Outlet or inlet holes were etched through the wafer with an anisotropic etch of ethylene diamine (22 mL), catechol (3 g), and H_2O (7 mL). This reaction was done with a reflux apparatus under nitrogen at the boiling temperature of the mixture, 118 °C, for approximately 10 hours. This was done in a fume hood in the chemistry department instead of the clean room. Once inlet or outlet holes were etched, samples were rinsed and returned to the microelectronics lab. The oxide mask layer was removed with BOE, and a new oxide layer of 0.5 micron thickness was grown to insulate the surface.

Electrode definition. For first-time construction of an electrode pattern, the steps described below were performed on flat SiO_2 samples to optimize procedures used before a 5 or 10 μm channel was encountered. It was found that without this preliminary experiment, it was difficult to determine the source of process problems. In most cases, the channel affected photoresist exposure times. Small featured patterns, for example an array with 5 μm wide fingers, sometimes were not possible to fabricate with an added step in the silicon. This was attributed to uneven distribution and thickness of photoresist in this channel, resulting in uneven exposure results. Also, lift-off metal deposition procedures where metal is deposited on top of patterned photoresist were attempted and found unsuccessful for fabrication of these detectors; metal did not adhere well to wafer surfaces in the channels.

After definition of flow channels, electrodes were then constructed along the length of the flow channels as shown in Figure 2-3. First, a thin film of an adhesion layer and then Au were deposited and patterned on wafer surfaces. Chromium (Cr) or Titanium (Ti) (15 nm) and then Au (250 nm) were layered onto the newly grown oxide layer using an electron beam evaporator. The under layer served to promote adhesion of the Au to the wafer surface. If Cr was used, samples were heated at 160 °C for two hours after deposition to promote adhesion. Once metallized, samples were again masked with positive photoresist (AZ 1375 or 1529 at 4000 rpm), soft-baked, and exposed through a reverse field mask which radiated the entire sample except for the desired electrode pattern. Exposure time for this step ranged from 30 seconds to 1.25 minutes. The electrode pattern was protected with photoresist, while the remaining Au was exposed

upon development for about 45 sec. This exposure time was more crucial than previous ones because if too long the electrode area was not well protected and disintegrated during etching. After development, samples were inspected visually under a microscope to check the integrity of the pattern. A post-bake to stabilize photoresist was done at 120 °C for thirty minutes. This bake is critical; unbaked photoresist would be dissolved during the metal etch. Also, temperatures above 135 °C resulted in photoresist being difficult if not impossible to remove after etching.

Exposed Au was etched with aqua regia (HCl and HNO_3 3:1). The under layer was etched with a commercial etchant for Cr available in the microelectronics laboratory, or BOE for Ti. Etch times for Au were between 1 and 2 minutes, while Cr or Ti etched in 10-20 seconds. Once electrodes were patterned, photoresist was removed with acetone and in some cases dilute sulfuric acid. The finished samples were cleaned with a foam tipped swab dipped in acetone to physically remove dirt or photoresist residue seen with a microscope. After rinsing with fresh acetone, electrodes were immersed and sonicated in isopropanol and DI water, each for 10 to 15 minutes. Samples were dried at 180 °C for thirty minutes. Flow channels were 85 μm wide and 2-7 mm long while detection electrodes were 50 μm wide and 2-7 mm in length. A scanning electron microscope (SEM) image of a finished electrode in a channel (on SiO_2) is shown in Figure 2-4.

Electrodes fabricated on Pyrex were prepared in a similar manner as those on SiO_2 with some exceptions. Electrodes defined on Pyrex were used as recycling electrodes and were made wider than detection electrodes. This made alignment of the two pieces easier than with a 50 or 100 μm electrode on the Pyrex, which was difficult to see. To make

wide (~350 microns) electrodes, Pyrex pieces were exposed in two steps of 20 seconds each. A light/dark edge of any mask was used to cover half of the Pyrex, exposing the second half. Samples were developed, rinsed, and surface dried with nitrogen gas. The second halves were exposed next, while protecting a portion of photoresist which defined the width of the electrode under the dark edge. A mask made for the desired width could also be designed to simplify this process. When Cr was used as an under layer during metal deposition, adhesion was not sufficient to make working electrodes on Pyrex. Therefore titanium was used exclusively as an under layer for all Pyrex electrodes. The Pyrex pieces were 1.25 cm x 1.25 cm x 0.05 cm thick, and ordered from Swift Glass if the pieces were solid. For some experiments, the Pyrex pieces had 360 μm diameter holes ultrasonically drilled through them (Bullen Ultrasonics) at the position indicated in Figure 2-1. These holes were used to attach fused silica capillaries for flow introduction of solution, while the large holes in silicon samples served as outlets. In other cases, smaller holes were used for attachment of capillaries, while outlets were at the top of the Pyrex piece (Figure 2-1).

To form completed flow-through cells as shown in Figure 2-1 B, Si and Pyrex portions of the cell were anodically bonded. The apparatus used for bonding is shown in Figure 2-5. Before bonding, pieces were aligned using a micromanipulator. The SiO_2 piece was fixed on the ground electrode. The micromanipulator held the high voltage electrode, a piece of stainless steel tubing, which held Pyrex pieces by vacuum through the tubing. SiO_2 pieces were placed on a stainless steel ground electrode on top of a hot plate. Pyrex pieces were positioned using the micromanipulator such that the two

electrodes were parallel opposed and the hole in each Pyrex piece was over the channel of the SiO_2 piece, then lowered to make contact. Once positioned, pieces were anodically bonded by first heating to 200-400 °C (heat setting 3.5 on hot plate) then applying 1000 V in conjunction with heating as described elsewhwere (51). For this work, the 1000 V power supply was operated with reverse polarity; the high voltage electrode touching Pyrex was biased at -1000 V while the electrode touching the SiO_2 was grounded. Bonding could be observed as a darkening and/or disappearance of interference patterns between the two pieces. Bonding formed an enclosed flow channel with Au electrodes separated by a distance defined by the channel depth which was 10 μm unless stated otherwise. This bonding procedure was unpredictable. For some batches of electrodes, bonding was fast (2-10 minutes) and successful for all samples. For other batches, little or no bonding was seen even after 1 hour. To test the bonding apparatus, plain pieces of Si or SiO_2 and Pyrex or microscope slide glass were bonded before actual microfabricated electrodes. Once bonding was observed between Si and microscope glass, real samples were bonded. Approximately 10% of the samples were ruined by sparking between the two electrodes; 10% were misaligned such that the two electrodes were not parallel opposed for the entire channel length, and 20% did not bond.

To introduce flow through cells, a fused silica capillary (25 μm i.d., Polymicro Technologies) was inserted into the drilled hole in the Pyrex piece and epoxied into place with Torr-Seal (Varian Vacuum Products) which takes 2 hours to dry at room temperature. Insertion of the capillary was done with the aid of a shop microscope. A micromanipulator was used to hold and position the capillary in the hole. A teflon holder

held samples vertical for this procedure. A flow of air was used through the capillary at all steps of epoxying to prevent clogging. Silver epoxy (Epo-tek 410E) was applied to contact pads of the microfabricated electrodes, which took 24 hours to dry at room temperature or 0.5 hour at 150 °C.

Apparatus and conditions. An Ensman EI-400 bipotentiostat was used for cyclic voltammetry and amperometry. Experiments were performed with a sodium saturated calomel electrode (SSCE) as the reference; all voltages are versus this reference. For testing assembled recycling detectors, the SSCE was positioned near the outlet hole in the Si portion of the cell. In some cases, cyclic voltammograms were recorded with a Goerz SE 790 X-Y recorder while amperometric traces were recorded with an ABB Goerz SE 120 flatbed recorder. In other cases, data acquisition for both procedures was accomplished with a National Instruments data acquisition board (AT-MIO-16f-5) and Lab Windows software written in-house.

Chronoamperometry was performed in the following manner. The electrochemical cell was filled with the analyte or buffer solution with 0.0 V applied to the detection electrode. Data collection was initiated, and after 10 seconds the potential was stepped to +0.3 V, and current response recorded. For dual electrode mode, the recycling electrode was maintained at -0.1 V for the entire experiment. For all samples, buffer was also analyzed with chronoamperometry to observe any effect of the recycling electrode on response.

The experimental apparatus for FIA is shown in Figure 2-6. Gas pressure was used to force solution through electrochemical cells via the attached capillary. FIA was

done by stopping the flow, exchanging the electrolyte vial for sample vial, applying gas pressure for a given time, then replacing the electrolyte vial and reapplying pressure. Single electrode amperometry was performed at +0.3 V. During dual electrode experiments, the recycling electrode was biased at -0.1 V. When dual electrode cells were tested, the preamplifier alligator clips were left attached to samples during the entire experiment to maintain good electrical connections. Recycling voltage was applied and turned off by attaching and detaching the preamplifier connector from the EI 400 back panel. This was done because it was determined that even when shut off, the channel held a voltage of 0.0 V. Detaching the preamplifier from the back of the potentiostat allowed voltage to be turned on and off to the recycling electrode without disturbing the preamplifier connection to the sample.

To determine the effect of heat and voltage required for anodic bonding on the electrode, some electrodes were analyzed by Auger spectroscopy at the University of Florida Major Analytical Instrumentation Center using a Perkin-Elmer PHI Auger Scanning Microprobe with an electron probe beam set at 5 kV. Since anodic bonding resulted in a permanent seal which did not allow access to the electrodes, samples that were analyzed with Auger were bonded with a modified procedure. Specifically, glass and Si pieces were aligned so that only small portions of the samples were in contact. After bonding, the pieces were separated with a diamond tipped scribe near the small portions of the surface which did form a seal. Although not completely bonded, electrodes were subjected to the same heat and voltage conditions as fully bonded cells.

Results and Discussion

Characterization of electrode surfaces. The electrode fabrication process described in the Experimental section resulted in an 80% yield for single electrodes and a 40% yield for complete detector cells testable for recycling. Less than perfect yields of single detectors resulted from over etching of the Au or under layer and lack of adhesion of the metal to the SiO_2 layer due to dust or other contaminants on the surface. In some cases electrodes would appear whole, but subsequent cleaning resulted in removal of Au from the surface. This was an indication that adhesion of metal to the substrate was not sufficient; a "good" electrode withstood cleaning procedures described in the last section. Not all electrodes were tested prior to anodic bonding. In most cases one electrode from a batch of 8 to 14 samples was tested with cyclic voltammetry to indicate that the batch was successfully fabricated and that the rest of the samples should be tested after bonding.

A possible factor limiting the success of the dual electrode cell fabrication yield was the application of high voltage and heat during anodic bonding. In some cases sparks caused the electrodes to be destroyed, as previously mentioned. Of particular concern was damage to electrode surfaces caused by anodic bonding. For example, passivation of electrodes is possible when underlying adhesion metal layer is heated and diffuses through or around the Au to form a non-electroactive oxide on the electrode surface (52).

To investigate the possibility of contamination or metal interdiffusion, Auger spectroscopy was used to determine the surface composition and depth profile of electrodes before and after anodic bonding. Electrodes which had not been subjected to anodic bonding conditions exhibited surface compositions of 20-60% carbon which could

be due to insufficient cleaning or contamination from air after cleaning. Before anodic bonding, oxygen and Cr contamination were minor (2% and 0% respectively).

After subjection to anodic bonding conditions, several changes were noted in composition of the electrodes as shown by the depth profile of an electrode on a SiO_2 substrate after anodic bonding illustrated in Figure 2-7. After anodic bonding, carbon contamination was reduced to <25% of the surface composition (3% in the example shown). Bonding increased the surface composition for Cr to 18% and oxygen composition to 38%. This presumably reflects formation of Cr oxides on the surface although Au oxide formation could not be ruled out. Contamination of the Au layer with Cr was not evident immediately below the surface. This suggests that Cr migrated by grain-boundary diffusion around the Au edges.

Surface contamination seen with Cr was mostly avoided by using Ti as an adhesion layer. An Auger depth profile for a bonded Au electrode with a Ti adhesion layer is shown in Figure 2-8. It was observed that surface contamination was <3% for Ti and oxygen after anodic bonding, much less than seen with Cr. Titanium was used exclusively as an adhesion layer after these experiments were performed.

To further investigate the effect of anodic bonding on microfabricated electrodes, cyclic voltammetry was performed in dilute sulfuric acid both before and after bonding. Oxidation and reduction of the Au surface in acidic solution results in characteristic surface waves which can be used to test a surface for Au electrode behavior (37). Figure 2-9 shows cyclic voltammograms of an electrode on a Pyrex substrate tested in 5 mM H_2SO_4 both before and after bonding. The post-bonding trace exhibited smaller peak

currents, which could be due to a smaller active area. This is in agreement with the likely passivation due to contaminants on the surface that was indicated by Auger spectroscopy. Potentials of Au oxide formation (1.4 V) and reduction (0.7 V) were unchanged in both pre- and post-bonding voltammograms indicating that although the active electrode area may be reduced, the surface continued to behave as Au electrochemically.

Voltammetric behavior of individual band electrodes. Characterization of microfabricated electrodes was also performed using cyclic voltammetry in 1 mM $Fe(CN)_6^{4-}$ both before and after anodic bonding. Figure 2-10 A shows the response of an unbonded electrode cycled in buffer solution and Figure 2-10 B shows the response of the same electrode when tested in analyte solution. The sigmoidal voltammogram is characteristic of a microelectrode with non-linear diffusion of analyte to the electrode. After anodically bonding a Pyrex cover piece over the electrode, a thin layer channel was formed with a 10 μm depth. Figure 2-10 C illustrates a voltammogram obtained after anodic bonding which is peak-shaped as expected for a thin-layer cell. In many cases voltammograms obtained from electrode cells after bonding were not thin layer, but resembled crosses between thin-layer and sigmoidal voltammograms; in some cases peak-shaped voltammograms were seen. A possible reason for this would be an incomplete seal between the two pieces, which would expose the electrode to a larger solution volume than desired, resulting in peak or sigmoidal behavior. A second possible cause was that the reference connection was made in a pool of solution at the outlet hole; a portion of electrode could be exposed to a non-thin layer of solution at this point. This initial CV

test of electrodes confined in flow cells was used to determine if both electrodes in the flow cell were working; if so, chronoamperometry and FIA were used to test the cell.

Amperometric response of single electrode detectors. Single electrode cells were used as amperometric detectors during FIA to assess the stability and sensitivity of their response as well as reproducibility between different cells. Current responses from repetitive injections of 0.1 mM $Fe(CN)_6^{4-}$ were recorded as a function of time to determine injection-to-injection reproducibility. A typical microfabricated electrochemical cell response to repetitive injections is shown in Figure 2-11. Electrodes typically exhibited 10-12% current losses during the first 15 min (not shown), followed by a stable response over 100 min of testing at a flow rate of 500 nL/min with injections every 7 min. These results are comparable to the 25% decrease in current response over a few hours reported by Anderson for flow injection studies at microfabricated Au arrays (53). After stabilization, a typical current maximum for a 0.1 mM injection at 500 nL/min was 26 nA, with a relative standard deviation (RSD) of 7% over the time tested.

Electrode response tended to decrease after storage in air. For example, one electrode retested after a 3-day storage showed responses 41% lower than those obtained on day 1. In some cases, the signal lost after storage could be regained by cycling the electrode potential between -0.4 V and +0.4 V at 200 mV/s for 5 minutes with the electrode in buffer.

Electrode to electrode variability, measured as the RSD for a current response to 0.1 mM 0.1 mM $Fe(CN)_6^{4-}$ at flow rates of 360 nL/min, was 15% (n = 4). A possible source of variation among the different electrodes was breaks along the electrode length

which would reduce the active area. After bonding, the detection electrode was covered from view by the recycling electrode; it was not possible to determine visually if the detector electrode was intact after the bonding procedure. Variations could have resulted also from misalignment and positioning of electrodes during anodic bonding which could result in a variable length of electrode confined to the flow channels. Passivation that occurred during anodic bonding could have also been a source of variation.

The root mean square (RMS) noise for single electrode detectors, measured over 60 s with low pass filtering at 5 Hz, was 3-10 pA. The detection limit, calculated as the concentration that would give a signal to noise ratio (S/N) of 3 for $Fe(CN)_6^{4-}$, was 50 nM in favorable cases. This detection limit is poorer than what is possible with carbon fiber electrodes. Part of the problem is higher noise per electrode area with microfabricated Au electrodes. For example, with 3 pA noise and electrode area of 2×10^{-3} cm^2, the microfabricated Au electrode has 1,200 pA noise/cm^2. A carbon fiber microelectrode with 9 μm diameter and 1.1 mm length has a nominal area of 3×10^{-4} cm^2 and a noise level of 0.08 pA (measured in our laboratory under similar conditions) resulting in 280 pA noise/cm^2. Higher noise levels in microfabricated electrodes relative to carbon fiber electrodes have been observed before (44). The higher noise levels may be attributed to surface contaminants in microfabricated electrodes and differences in electrode materials.

Recycling studies of dual electrode cells. After characterization of single electrode cells, the recycling ability of dual electrode cells we investigated with chronoamperometry and FIA. Chronoamperometry was used as an initial indicator of a dual cell's ability to recycle. Since it is a static technique, chronoamperometry gave an estimate of the largest

amount of recycling possible. A typical chronoamperometric response to 0.1 mM ferrocyanide is shown in Figure 2-12. In this case the response of the detector using both the detection and recycling electrodes was 25 times larger than that of the single electrode case. If an electrochemical cell did not show recycling (i.e. a larger signal for dual electrode response) then it was not tested further.

Samples showing recycling were then tested with FIA. Flow injection results from a dual electrode detector, compared to that obtained with the recycling electrode disconnected, are shown in Figure 2-13. The detector cell exhibited a 22-fold enhancement of signal in the dual mode over that of a single electrode with the flow rate at 37 nL/min. This agrees fairly well with random walk simulations developed in Chapter 4, which predicted a 16-fold signal enhancement at this flow rate. Differences between simulation and experiment could be due to fluctuations or derivation from the calculated flow rate. Larger enhancements were possible with smaller gaps as illustrated by the results in Figure 2-14 from a cell with 5 μm spacing between the electrodes. In this case, the flow rate was 50 nL/min and > 60-fold signal enhancement was achieved relative to single electrode operation.

The dual electrode cells were tested to determine the effect of flow rate on signal enhancement. Signal enhancement was defined as the ratio of oxidative current using both electrodes to that with just the detector electrode connected. For experimental results, signal enhancement was calculated as the ratio of the peak current obtained by FIA for dual electrode operation to that in single electrode operation. As expected, increasing the flow rate decreased the residence time in the cell and decreased the amount of signal

enhancement seen. The flow rate dependency was in good agreement with that predicted by the random walk model developed in Chapter 4 for a cell with a 10 μm gap (Figure 4-4). These results indicate that the microfabricated cells can successfully be used as recycling detectors in the range of flow rates necessary for microcolumn separations.

Although the signal increases are promising, a noise increase which reduced the S/N gain was observed in most cases upon switching from single to dual electrode detection. For example, in Figure 2-14, the noise increased 8-fold as the signal was increased by 60-fold for dual electrode operation relative to single electrode operation. The increase in noise was variable with an average of 5.6 ± 5.0 over single electrode operation. A fraction of the noise may be related to difficulties in making good connections as the noise varied if electrodes were disconnected and reconnected. Noise varied with many parameters, such as the size of the reference electrode solution drop and the position of the alligator clamp. Other sources of noise include potentiostat electronics during dual-electrode operation and noise current caused by the low impedance cell (8). This latter source of noise can be reduced by the use of appropriate circuitry as described in Chapter 3.

The results demonstrate successful microfabrication of single and dual electrode cells having volumes compatible with capillary LC and CZE. Predicted signal enhancements of over 60-fold were achieved in electrochemical cells at flow rates typical of capillary separation methods. A potential problem in the fabrication procedure presented here is the use of anodic bonding. While providing a good seal, anodic bonding also leaves contamination on the electrode surface which may increase noise levels and

decrease the active area, and could possibly weaken the electrodes. Lower temperature bonding methods could be developed. Other important areas for improvement include use of electrode materials, especially carbon, that are more useful analytically. This is investigated in Chapter 3.

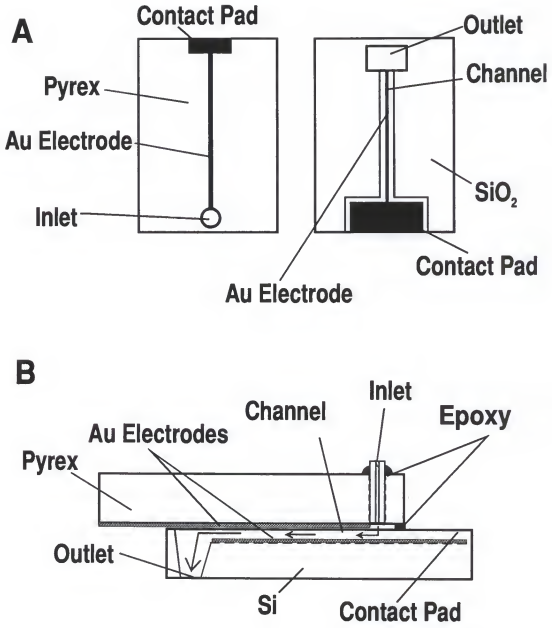

Figure 2-1. Design of recycling electrochemical detector. (A) Top view of finished electrodes on Pyrex and SiO_2. (B) Cut away view of assembled detector. Arrows indicate flow path. Dimensions given in text.

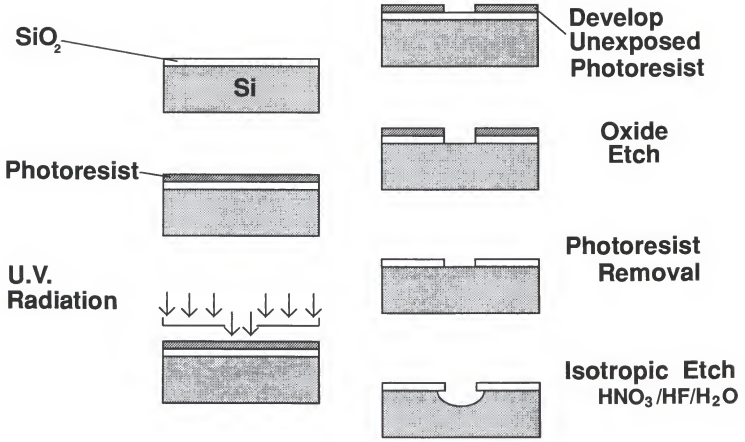

Figure 2-2. Photolithographic steps used to etch channels into silicon surface. The oxide mask is then removed with a buffered oxide etch and a new layer of oxide grown.

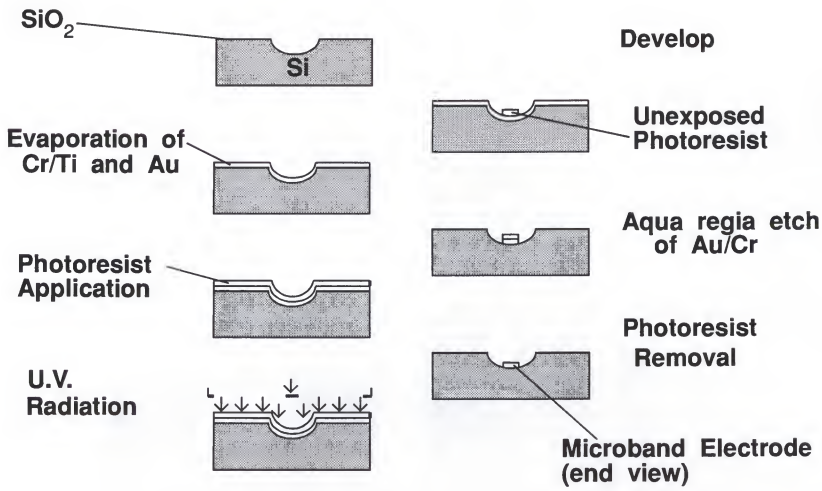

Figure 2-3. Deposition and etch steps used to define gold band electrodes. Cr or titanium was used to facilitate gold adhesion to the silicon dioxide surface.

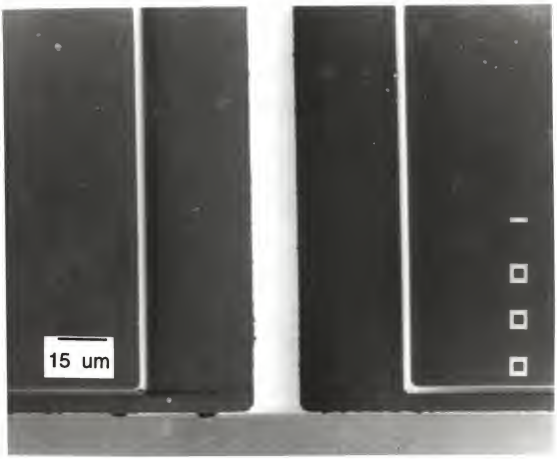

Figure 2-4. Scanning electron micrograph of a Au microband electrode (15 μm wide). The electrode is located in a channel (90 μm wide x 5 mm length) which has been etched into the surface of the SiO_2. The bright area in the center is the Au electrode which connects to the larger contact pad near the bottom of the photograph. Magnification is 1000x. Electrodes actually used for electrochemical experiments were 50 μm wide.

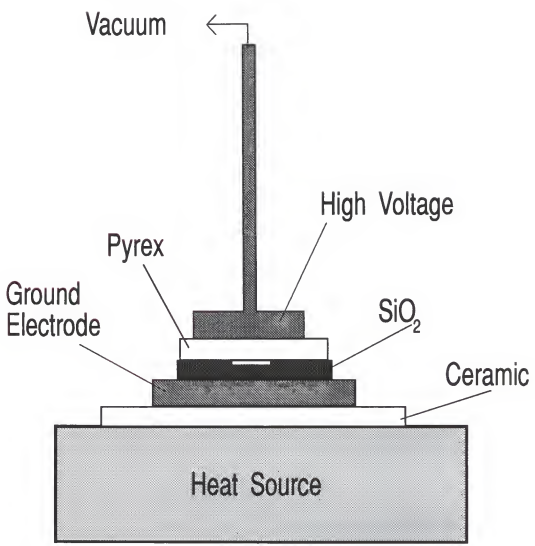

Figure 2-5. Diagram of the experimental apparatus used for anodic bonding. The high voltage electrode was a piece of stainless steel tubing through which vacuum was applied. The vacuum was used to hold the Pyrex electrode while positioning it over the SiO_2 electrode. The SiO_2 electrode was placed on the ground electrode, which was a piece of stainless steel. The ground electrode was placed on a ceramic square which was itself placed on a hot plate. Connections from the high voltage power source to the electrodes were made with alligator clips.

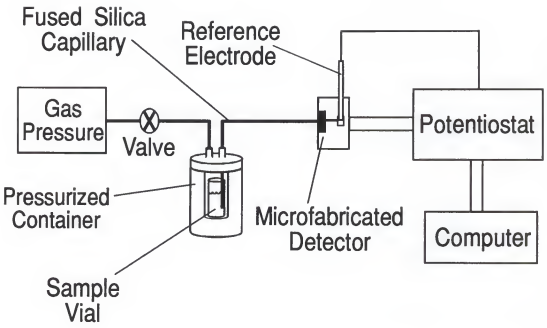

Figure 2-6. Diagram of the experimental setup used in flow injection analysis experiments. Gas pressure was used to force sample or buffer solution from a high pressure bomb through a fused silica capillary. The capillary was epoxied to the microfabricated detector. A reference connection was made at the outlet hole of the detector. A potentiostat applied a constant potential to the electrode. Current was recorded and processed on a personal computer.

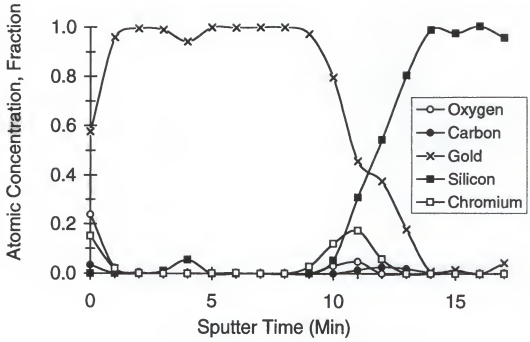

Figure 2-7. Auger spectroscopy depth profile of a Au electrode with a Cr underlayer on an SiO_2 substrate after subjection to anodic bonding conditions. Atomic composition fraction was plotted as a function of sputter time for each element. Total depth approximately 265 nm.

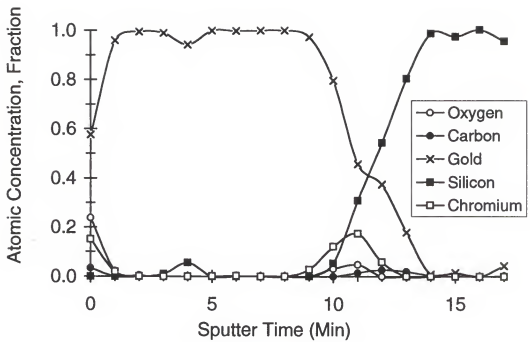

Figure 2-8. Auger spectroscopy depth profile of a Au electrode with a Ti underlayer on an SiO_2 substrate after subjection to anodic bonding conditions. Atomic composition fraction was plotted as a function of sputter time for each element. Total depth approximately 265 nm.

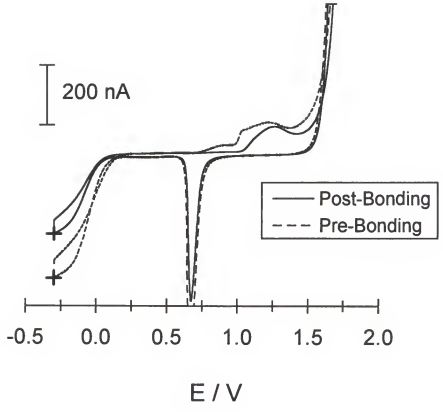

Figure 2-9. Cyclic voltammograms of a Au band electrode tested in 5 mM H_2SO_4 before and after anodic bonding. The anodic peak at 1.4 V indicates Au oxide formation while the cathodic peak at 0.7 V indicates Au oxide reduction. Crosses indicate the beginning of the scan and the zero current level.

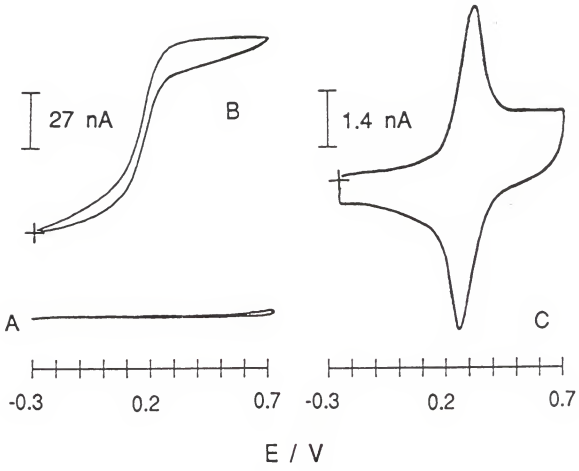

Figure 2-10. Cyclic voltammograms obtained on microfabricated band electrodes in 1 mM $Fe(CN)_6^{4-}$ with 0.1 M Na_2SO_4 as the background electrolyte. (A) blank; (B) uncovered electrode immersed in solution; (C) bonded (or covered) electrode (electrode is different from that used in (A) and (B)). Scan rate was 50 mV/s. Crosses indicate the beginning of the scan and the zero current level.

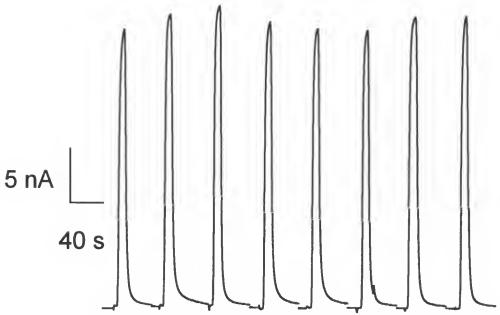

Figure 2-11. Current response of single electrode detector to repetitive injections of 0.1 mM $Fe(CN)_6^{4-}$. Injections were made 7 minutes apart. The flow rate was 600 nL/min. The detection potential was 0.3 V.

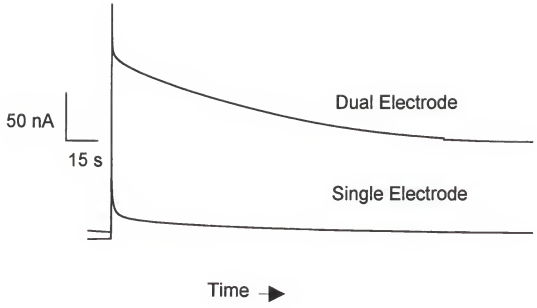

Figure 2-12. Chronoamperometric response of dual and single electrode detection modes. Potential at the detection electrode was initially 0.0 V, then stepped to 0.3 V after 10 seconds. The recycling electrode was biased at -0.1 V at all times. The solution in the detector was static for these experiments.

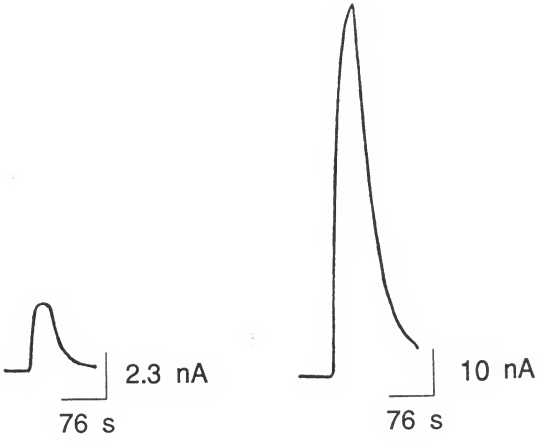

Figure 2-13. Flow injection current-time traces for injections of 0.1 mM $Fe(CN)_6^{4-}$ detected by a dual electrode cell with and without the recycling electrode connected. The flow rate was 37 nL/min. The electrochemical cell had a gap of 10 μm between the electrodes.

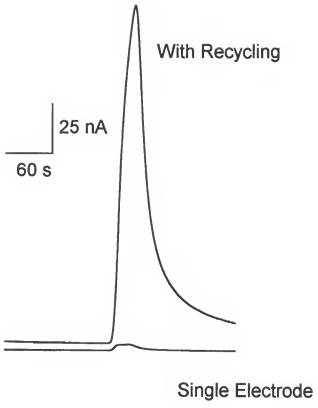

Figure 2-14. Flow injection current-time traces for injections of 0.1 mM $Fe(CN)_6^{4-}$ detected by a dual electrode cell with and without the recycling electrode connected. The electrochemical cell had a gap of 5 μm between the electrodes and the flow rate was 50 nL/min.

CHAPTER 3
MODIFICATIONS AND IMPROVEMENTS OF THE PARALLEL OPPOSED RECYCLING ELECTROCHEMICAL DETECTOR

Introduction

The goal of the work presented in this chapter was to improve the performance of parallel opposed microfabricated ECDs. As described in Chapter 2, detectors with 5 μm channels between two electrodes enhanced the measured signal in FIA by as much as 60-fold. Although significant, several limitations were encountered during the testing of parallel opposed cells. First, an increase in noise levels was observed when detection was changed from single to dual (recycling) mode, reducing the effect of enhanced signal on S/N. Also, single Au electrode detectors exhibited noise levels which were 5-fold higher than carbon fiber detectors, the most widely used detector for microcolumn separations. Finally, experiments were limited to Au electrodes, which exhibit a narrower potential range and therefore detect a smaller range of compounds than carbon fiber detectors.

This chapter addresses methods used to overcome these limitations. Reduction of noise observed during dual electrode detection was accomplished through the use of a custom built potentiostat switching circuit which reduced noise by switching the working electrodes in and out of connection with the potentiostat. Also, individual Au electrodes were replaced with microelectrode arrays to reduce area-dependent noise while maintaining signal currents similar to solid electrodes. To increase the applicability of

recycling detectors and possibly reduce noise levels, carbon films were investigated as replacements for Au as the electrode material. For each limitation described above, this chapter will present a brief introduction which includes the proposed solution, followed by description of experimental procedures used to test the proposed solution, and finally results obtained and conclusions drawn from them.

Potentiostat Electrode Switching Circuit

Although the 20-60-fold signal increases observed with parallel opposed recycling detectors in Chapter 2 are significant, the noise increase observed in many cases upon switching from single to dual electrode detection reduced S/N gain (Figure 3-1). For example, while signal was increased by 60-fold for dual electrode operation relative to single electrode operation (Figure 2-14), noise increased 8-fold, reducing the net gain in S/N increase from 60 to 8. The magnitude of the noise increase varied with most cells, with an average increase of 5.6 ± 5.0 (n=27) over single electrode operation.

A significant source of noise observed during dual electrode detection can be attributed to potentiostat electronics and was explained by Purdy and Weber in their investigation of recycling electrochemical detection (8). That work determined that a large contributor to noise in measured currents is voltage noise in the current to voltage converter (Figure 3-2). This voltage noise generates a current noise through the cell impedance. If a cell has low impedance, the equivalent current noise measured for a given voltage noise will be high. Parallel opposed detector electrodes are separated by a thin layer of solution which has low resistance, resulting in a large noise current between them (Figure 3-2). Purdy and Weber proposed to reduce noise currents by switching the

working electrodes in and out of electrical contact with the potentiostat. When the electrode(s) are out of electrical contact, current to voltage converter current noise is zero. More specifically, if σ_{dc}^2 is the experimental noise power in a normal potentiostat, in the switched case the noise will be:

$$\sigma_{sw}^2 = \sigma_{dc}^2(t_{on}/(t_{on} + t_{off})) + \sigma_{ex}^2 \qquad (1)$$

where t_{on} is the length of time the switch (electrode) is connected, t_{off} is the length of time the switch is open, and σ_{ex}^2 is the excess noise created by switching. For a small duty cycle ($t_{on}/(t_{on}+t_{off})$) the measured noise may be lower than in normal operation, because the noise is zero during the time the switch is open.

An improved S/N ratio is expected for duty cycles which do not severely reduce the signal observed. When the electrode is out of connection, the potential difference has time to relax across the double layer of solution. When the electrode is switched off, potential at the electrode surface can still induce redox reactions until it droops below the redox potential of the analyte. Charge will build up on the electrode surface until the switch is closed, allowing current flow, when the resulting signal can be measured. A slow relaxation of potential difference across the double layer is necessary to maintain potential at the electrode surface. Potential relaxation, or "droop", increases with the length of time the switch is open, as does resulting charging and background currents when the switch is closed and the electrode returns to the applied potential. This indicates that short sampling intervals (fast switching) would possibly result in the lowest noise levels.

For this project, a potentiostat switching system was built by Ensman Instrumentation which is used in conjunction with the regualar EI-400 potentiostat.. The circuit was based on the circuit built by Purdy and Weber but modified for microelectrodes. The effects of switching on the performance of parallel opposed recycling detectors were investigated with both single and dual electrode detectors.

Experimental. Reagents and solutions were prepared in the same manner as described in Chapter 2. Fabrication procedures for flow-through recycling electrochemical detectors were the same as described in Chapter 2, with channel depths (distance between electrodes) ranging between 6 and 9 μm. Initial testing of the samples was done with an Ensman EI-400 bipotentiostat for cyclic voltammetry, chronoamperometry, and preliminary FIA amperometry. Experiments and data collection using the EI-400 were performed as described in Chapter 2. Before testing with the EI-401 switching system, a flow rate was chosen with the EI-400 which allowed significant recycling (> 5 x signal enhancement) in a reasonable analysis time (< 5 min) for a given sample. FIA procedures using the EI-401 were similar to those for the EI-400 except that additional current measurements were made for injections at different sample rates and duty cycles tested.

Switching of the working electrodes in and out of contact was accomplished using the EI-401 potentiostat headstage switching system. The EI-401 dual channel headstage replaces the preamplifiers normally used with the EI-400. The EI-401 uses a monolithic fabricated integrator to implement a high gain, continuous, current to voltage function the same as the standard EI-400 preamps with the added feature that the electrodes can be

switched in and out (Appendix A). An important feature of the switching system is that circuitry was incorporated to permit data acquisition (integration cycle triggering) to be synchronized to the 60 Hz AC power line. Therefore, if the amperometric inputs of the EI-401 headstage pick up noise current from any source derived from the AC power line, the signal at the output will remain fixed in amplitude for each data point or repeating series of data points.

The sampling rate determines the cycle interval or rate of integration/switching cycles per second. The rates are integral multiples of the AC line frequency from 3 Hz (333 ms) to 2400 Hz (417 μs) which can be set with a 12-setting dial control. (Table 3-1). The integration time, or the time that the working electrode is connected, can be continuously varied from 5 μs to 100 ms within a given sampling interval. The duty cycle is defined as the ratio of the integration time to the sampling interval. For this work duty cycles of 0.02 and 0.5 were chosen.

Table 3-1. Sample Intervals for EI-401 Switching System

Dial Setting	Sampling Rate (Hz)	Interval (ms)	Sampling Rate per AC Line Cycle
1	3	333	0.05
2	6	167	0.1
3	12	83.3	0.2
4	24	41.7	0.4
5	30	33.3	0.5
6	60	16.7	1
7	120	8.33	2
8	240	4.17	4
9	300	3.33	5
10	600	1.67	10
11	1200	0.833	20
12	2400	0.417	40

Results and discussion: single electrode detectors. The operation of the EI-401 potentiostat headstage switching system was initially characterized using single electrode detectors during FIA. Signal and noise levels were measured at different sampling intervals and duty cycles for injections of $Fe(CN)_6^{4-}$ to determine which combination resulted in the highest S/N values. Typical responses are plotted in Figure 3-3 for a duty cycle of 0.02. The measured signal increased with an increase in the sampling interval in a non-linear but reproducible fashion for single electrode samples. Noise levels also increased with the sampling interval but not in proportion with the signal. The mean RMS noise levels (measured over 60 seconds at a 5 Hz bandwidth) at the shortest sampling interval (417 μs) were 4.1 ± 3.7 pA (n = 11), smaller or comparable to EI-400 single electrode noise levels of 11.5 ± 5.5 pA/cm (n = 14). At the longest intervals tested (42 ms) The mean RMS noise was 1533 pA ± 1718 pA, larger than noise levels observed with normal EI-400 operation.

As shown in Figure 3-3, the combined effects of switching on signal and noise levels resulted in a S/N maxima at a sampling interval of 4.2 ms. A maximum 10-fold increase in S/N over the EI-400 was observed; the mean S/N increase was 1.3 ± 0.8. At sampling intervals longer than 8.3 ms, the S/N levels fell below that observed with the EI-400 due to the large noise increases (Figure 3-3). However, the S/N increase observed at 4.2 ms indicates that it is feasible to improve the sensitivity of the EI-400 by using the switching system with single electrode detectors. The increases in signal and noise with sampling interval are expected from the increased amount of time the electrode is out of connection with the circuit, as explained earlier.

The effect of changing the duty cycle on the S/N ratios within a given sampling interval was also investigated with single electrode detectors. Equation (1) indicates that the larger the duty cycle, the larger the noise level will be for a given sampling interval. However, the longer the electrode is kept at the maximum potential (i.e. longer duty cycle), the larger the amount of signal current measured. For single electrode samples, the effect of changing the duty cycle was not reproducible within a given sampling interval or from sample to sample. In some cases the signal increased by as much as 200 % when the duty cycle was increased to from 0.02 to 0.5; in other cases a decrease was seen (up to 45 %), and in other cases no signal change was observed. The effect of changing the duty cycle on the noise levels was similarly inconsistent, as was the resulting effect on the S/N ratio. This indicates that during future experiments with the switching circuit, the duty cycle must optimized empirically. Also, additional values of duty cycles could be tested to determine if there is an optimum value.

Results and discussion: dual electrode detectors. The objective of the electrode switching system was to reduce or eliminate noise increase during dual electrode recycling detection. This noise reduction, in combination with signal enhancement achieved with parallel opposed recycling detectors, should result in increased S/N ratios over the EI-400. Signal and noise levels were measured with dual detectors at different sample intervals and duty cycles for injections of $Fe(CN)_6^{4-}$. The S/N values were compared to those obtained with no switching (Figure 3-4). In dual electrode detection mode, a sampling interval of 417 μs was found to exhibit the smallest noise levels and highest S/N levels. This result differs from those obtained by Purdy and Weber (8), who observed a maximum S/N ratios

at a sampling intervals of ~4 ms. This could possibly be attributed to the difference in the electrode areas. Their electrodes were 15 cm^2 while the electrodes in this work are approximately 1000 times smaller. The larger area electrodes probably do not "droop" as fast as the electrodes used here, and therefore a longer switching time could be used without large increases in background and noise.

The combined effects of lowered noise levels and increased signal due to analyte recycling resulted in a S/N increase of 10-fold over single electrode detection as shown in Figure 3-5. The signal and noise levels are shown for both EI-400 single and dual detection modes (no switching) as well as dual detection with the EI-401 at a sampling rate of 417 µs (duty cycle 0.5). Figure 3-5 A shows the response and RMS noise of a single electrode to injections of 10 µM $Fe(CN)_6^{4-}$ without switching. Figure 3-5 B shows the increased response and noise levels due to electrochemical recycling with the same detector in dual detection mode without switching. The signal was enhanced 6-fold by recycling, but the noise level also increased by 20-fold. Figure 3-5 C shows the response and noise level of the same detector in dual mode with the EI-401 at a setting of 417 µs sampling interval. The noise level is reduced to approximately the same level observed with the single electrode, resulting in an overall increase in S/N of 10 (over EI-400 single electrode detection). As described for single electrode detectors, the effect of changing the duty cycle from 0.02 to 0.5 on S/N ratios for dual electrode operation was inconsistent; therefore the duty cycle must be optimized for each sample.

As reported in Chapter 2, the LOD achieved with parallel opposed dual detectors was 50 nM in favorable cases. The response to an injection of 10 nM $Fe(CN)_6^{4-}$ detected

in dual electrode mode with sampling interval of 417 μs is shown in Figure 3-6, indicating that the LOD possible with the switching circuit is improved over that observed with no switching. The increased S/N values obtained with the EI-401 resulted in a LOD of 1-5 nM for $Fe(CN)_6^{4-}$. A calibration curve for $Fe(CN)_6^{4-}$ is shown in Figure 3-7. The response was linear from 100 nM to 100 μM.

The use of the EI-401 switching system at a sampling interval of 417 μs resulted in a 10-fold increase in S/N over that achieved with a single electrode. The detectors tested in this work had channel depths of 6-9 μm compared to the 5 μm depths which exhibited the 60-fold signal increase in Chapter 2. Therefore it is expected that further improvements in S/N can be obtained with the use of 5 μm channels which recycle analyte to a larger extent than those tested here. However, even with the 6-9 μm channels tested the switching system improved the LOD for $Fe(CN)_6^{4-}$ by at least 10-fold over single electrode detection. This improved sensitivity is promising for application of these detectors to microcolumn separation techniques.

Gold Array Electrodes

A significant factor limiting the LOD for the microfabricated detectors was higher noise levels per area for Au electrodes over carbon fibers. As stated in Chapter 2, the root mean square (RMS) noise for single electrode detectors, measured over 60 s with low pass filtering at 5 Hz, ranged from 3-10 pA with an average of 6.0 ± 3.3 pA. This corresponds to noise levels approximately 5-fold higher than a carbon fiber. One possible source could be related to difficulties in making good electrical connections to the electrodes; the noise varied if the electrodes were connected and reconnected to the

preamplifier. Other possible sources of noise could be surface contaminants from processing (incomplete cleaning), anodic bonding, adsorption of solution components, or fluctuations in the working electrode-reference electrode potential difference.

Although there are many equations available to calculate signal currents, noise is less understood (54). Theoretical analysis shows that noise will decrease with electrode area to a point and then will be constant (55). Array electrodes exhibit increased S/N ratios over solid electrodes. Array fingers which are spaced closely together allow diffusion layers of adjacent fingers to overlap, resulting in signal levels comparable to solid electrodes. Elimination of electrode area between fingers results in increased mass transport due to nonlinear diffusion to the edges (56) as well as reduced noise compared to a solid electrode of similar dimensions, resulting in increased S/N ratios. Simulations described in Chapter 4 predict approximately a 2-fold increase in S/N over a solid electrode for a recycling parallel opposed detector with a 50 μm wide array consisting of 5 μm array fingers separated by 5 μm gaps. Gold microband electrode arrays were fabricated to investigate the S/N increases possible.

Experimental. The fabrication procedure for array electrode detectors was similar to that described for parallel opposed detectors in Chapter 2 with the following exceptions. Two patterned masks were made for definition of electrode arrays; one had 5 μm fingers separated by 5 μm gaps, and the other had 10 μm fingers separated by 5 μm gaps. The total width of arrays were 45 and 55 μm, respectively. Minimum width of fingers was limited by photolithography equipment and photoresist characteristics; smaller dimensions have been fabricated by others with different instrumentation (39). Etching of

flow channels and deposition of metal layers were done as described in Chapter 2. If arrays were fabricated in the silicon flow channel, exposure time of the photoresist (AZ 1529) to define the array pattern was critical. It varied between batches of electrodes, ranging between 23-26 seconds. Initially, photoresist patterns for 5 μm finger arrays were unstable and did not withstand aqua regia etching. This problem was attributed to uneven distribution of the photoresist in the flow channel, which lead to non uniform patterns. To promote photoresist adhesion and stability, Au coated samples were cleaned after evaporation in boiling acetone, sonicated in methanol and DI water, and then dried before photoresist application. The post-exposure baking temperature was adjusted to 130 ^{o}C to strengthen the resist.

Under these conditions the photoresist was stable during aqua regia etching. However, when the photoresist was removed it was observed the gold had been underetched, with most array fingers broken or very thin (~1 μm) with rough edges. A pirhanna etch cleaning of the gold (see Chapter 2) before photoresist application was used to improve the protecting ability of the photoresist. However, Au was again undercut during etching, resulting in very thin array fingers. Due to these problems, the yield of intact 5 μm arrays was only 5-10 %. The smallest array dimension reproducibly fabricated in a channel was 10 μm finger widths with 5 μm gaps.

To alleviate problems associated with uneven distribution of photoresist in the flow channel during electrode patterning, array electrodes were fabricated on the flat Pyrex portion of the detector. In this case a solid recycling electrode in the silicon flow channel was used. Arrays on Pyrex were prepared similar to SiO_2 array pieces: evaporation of

Au/Ti, cleaning, and photoresist (AZ 1529) application. The exposure time was optimal at approximately 23 seconds, which was sufficient to give 5 μm finger resolution. After fabrication, Pyrex-based array electrodes were anodically bonded to SiO_2 counterparts. However, the 50 μm wide arrays were difficult to see and align with SiO_2 electrodes during anodic bonding, resulting in electrodes which were either totally or partially misaligned. For this reason array construction was done exclusively on SiO_2 with a wide recycling electrode on Pyrex, and was limited to 10 μm wide fingers. Array samples were tested with CV, chronoamperometry, and FIA.

Results and discussion. To assess the noise characteristics of single array electrodes, the RMS noise was measured over 60 seconds at a 5 Hz bandwidth during FIA in the same manner as the solid electrodes. The noise measured per length of electrode was compared to the noise levels of solid single electrodes of the same total width. A sample of the data is shown in Figure 3-8. The average noise per length ratio of the array samples tested was 4.4 ± 1.0 pA/cm ($n = 5$), compared with an average of 11.5 ± 5.5 pA/cm for solid electrodes ($n = 14$). The decrease in noise was 2.6-fold for array electrodes compared to solid ones. However, the LOD did not improve in all cases as the noise decreased. An LOD of 20 nM for ferrocyanide was achieved for one sample, an improvement over the 50 nM limit observed for solid electrode samples. A second sample exhibited the same detection limit as the solid electrodes, while a third was less sensitive than either the solid or array electrodes, with an LOD of 300 nM.

Chronoamperometry and FIA were used to test array samples in the dual electrode mode to investigate their recycling characteristics. Two samples tested exhibited

recycling. Signal enhancement of 2-fold was seen for Sample 1 and an 8-fold signal enhancement was seen for Sample 2 for $Fe(CN)_6^{4-}$ detection in dual electrode mode compared to the single electrode case. As with the solid electrode detectors, a noise increase was observed for arrays during dual electrode (recycling) mode. Sample 1 exhibited a 5-fold increase in noise over a single electrode, while Sample 2 a 20-fold increase. Improved fabrication processes and testing of more samples are necessary to determine if Au arrays will lead to lower limits of detection for parallel opposed recycling detectors.

Carbon Film Electrodes

Replacement of Au with a carbon film as the electrode material was another method investigated to improve the performance of the recycling electrochemical detectors. The objective was to fabricate carbon film electrodes which have wider application than the gold parallel opposed detector cells. Various forms of carbon have played an important role in solid electrode development, making it the most widely used material in electroanalytical chemistry and LC-ECD (57). Slow oxidation kinetics of the carbon surface result in a wide useful potential window, particularly in the positive direction. This is an important advantage over platinum and mercury, which exhibit significant oxidation background levels (57). The wide potential window (-1.0 V to +1.0 V) allows the detection of more types of molecules, making carbon more versatile than noble metals. In addition, carbon exhibits a rich surface chemistry, making a variety of chemical derivatizations possible which can influence reactivity. Also, as previously mentioned, coworkers in this laboratory have observed lower noise levels for carbon fibers

than Au electrodes. Carbon film electrodes, therefore, could increase the sensitivity of the recycling detectors as well as the applicability to more molecules.

Three types of carbon film deposition techniques have been published: 1) thermal decomposition of low molecular weight aliphatic hydrocarbons, 2) electron beam evaporation or sputtering of carbon, and (3) pyrolysis of high molecular weight organic compounds onto substrates at high temperatures (58). All three techniques have been used to fabricate electrodes. Recently, pyrolysis of polyaromatic hydrocarbons was applied to the construction of carbon film interdigitated array electrodes which were used as detectors for HPLC (59). This technique, originally described by Kaplan and coworkers (Figure 3-9), was adapted by us for construction of both band and interdigitated array carbon film electrodes (60) (Figure 3-10).

Experimental. Carbon vapor deposition (CVD) of carbon films was achieved by pyrolysis of 3,4,9,10-perylenetetracarboxylicdianhydride (PTDA) under vacuum. A diagram of the deposition apparatus is shown in Figure 3-10. A 100 cm length, 2 cm diameter quartz furnace tube was modified with a quartz ball joint (size 75/50), while a borosilicate glass socket of the same size was sealed at the end and modified with a vacuum stopcock. Silicon dioxide samples were placed on a quartz boat and positioned near the center of the tube. Approximately 0.6 g of PTDA was placed in a quartz boat and positioned such that it would be just outside the heating element of the furnace. The joint was clamped, and the tube pumped down to 10 mTorr. The furnace heating element was initially set at 350 °C, below the sublimation temperature of the PTDA. Once evacuated, the tube was inserted into the furnace and the temperature adjusted to 900 °C,

requiring 1 hour to reach a stable temperature. The quartz tube was then pushed approximately 0.5 cm every 25 minutes into the furnace to sublime the PTDA. This process was repeated until the entire length of the boat holding the PTDA was inserted into the heating element of the furnace. This typically required between 3 and 4 hours. After deposition, the furnace was shut off and allowed to cool to room temperature for 3 hours.

The resulting samples with carbon films were cleaned in 0.1 M NH_4OH with sonication for 10 minutes, then rinsed in boiling trichloroethane for 10 minutes. They were sonicated in acetone then methanol for 10 minutes each, rinsed with DI water, and dried at 180 °C for 30 min. Photoresist was applied by spin coating (AZ 1529) and soft-baked in the same manner as for gold electrodes. Two types of electrodes, band electrodes in silicon channels and IDAs, were fabricated with carbon films. For band electrodes, the exposure time of the photoresist to define the electrodes (25-30 s) and the hard bake temperature (120 °C) were the same as for the Au detectors in Chapter 2. The IDAs were fabricated on flat silicon dioxide pieces which had two ansiotropically etched holes in the surface for the inlet and outlet. Exposure time for these samples was 25-26 seconds. IDA masks had 5 μm fingers for both electrodes with a 5 μm gap between them. IDA samples were hard baked at an elevated temperature of 130 °C to stabilize the photoresist during the etching step.

A reactive ion etcher was used to define electrodes after photoresist patterning by etching the carbon film. This instrument utilized an oxygen and argon plasma (ratio 2:1) to selectively etch the exposed carbon areas. The photoresist was either unaffected or was

etched at such a slow rate that it was negligible. During etching the pressure was set at 400 mTorr, and the radio frequency (RF) power was 200 mW. Carbon was etched first from the back of the samples by placing them face down on the sample holder, then turned, and the photoresist-patterned carbon was etched. The samples were etched in 1 minute increments and the progress monitored; etching time varied from 1 to 5 minutes depending on the batch and sample. Cleaning and anodic bonding of the carbon electrodes after etching was the same as described in Chapter 2.

For carbon IDA samples fabricated on SiO_2, flow channels were etched into the surface of the Pyrex pieces. To fabricate channels, the Pyrex pieces were pirhanna etch cleaned and dried at 180 °C. Ti (15 nm) and Au (250 nm) were evaporated onto Pyrex using electron beam evaporation. In this case, the metal layers were an etch mask for Pyrex. Photoresist (AZ 1512) was spun onto the Au surface and soft baked. Flow channels (80 μm wide by 1 cm in length) were exposed through a mask for 20 seconds, and the samples developed, rinsed, and hard baked. The Au/Ti mask was etched with aqua regia where photoresist was removed, exposing the Pyrex surface. The Pyrex was etched using either BOE or a mixture of $HNO_3/HF/H_2O$ in a ratio of 20:14:66 (61). The metal mask was removed using aqua regia. Etched channels were 5 μm deep, 80 μm wide at the bottom and 150-250 μm wide at the top.

Results and discussion. The thickness of the chemical vapor deposited carbon films was highly variable. The amount of carbon deposited on the samples was dependent on the distance between the sample and chemical boats during deposition (Figure 3-11). Best results were obtained when the sample boat was within a few cm of the end of the

chemical boat. If the sample boat was too far removed from the chemical boat, carbon pyrolyzed on the sides of the furnace tube and did not reach the samples. Another problem was encountered if the chemical was introduced too quickly into the heating element of the furnace; decomposition occurred and the samples covered with black soot. Successful pyrolysis without decomposition resulted in carbon films with a silver-grey mirrored finish. The carbon film thickness, measured with profilometry after etching, varied from 100 nm to 350 nm from batch to batch and also within a single batch, depending on where a piece was positioned in the sample boat. Carbon band electrodes were of the same dimensions (50 μm wide x 5-7 mm in length) as microfabricated Au electrodes.

The voltammetric behavior of the carbon band electrodes was tested with cyclic voltammetry. A typical result for a carbon band electrode in 100 μM in $Fe(CN)_6^{4-}$ is shown in Figure 3-12. The sigmoidal voltammogram is characteristic of a microelectrode with non-linear diffusion of analyte to the electrode, as observed with gold band electrodes in Chapter 2. 67 % of the band electrodes tested showed similar responses to $Fe(CN)_6^{4-}$, while the rest showed little or no response. Current levels were comparable with those observed with gold electrodes. These results indicated that the vapor deposited carbon material was behaving as an active electrode surface, and fabrication of dual parallel opposed electrode cells was attempted.

To fabricate dual electrode cells, Pyrex samples were pyrolyzed in the same manner as SiO_2. However, the CVD procedure was not suited for carbon deposition onto Pyrex samples; the temperature used (900 °C) was above the softening point of the glass,

resulting in curved samples. Alternatively, Au electrodes were used on Pyrex as the recycling electrode for the parallel opposed detectors. However, the carbon electrode samples did not bond properly. For carbon band samples which did bond, the carbon appeared melted or broken in one or more spots. For this reason, no amperometry data or noise characteristics were obtained for carbon band electrodes.

To construct a recycling ECD with both electrodes made of carbon, IDAs were constructed on SiO_2 flats (Figure 3-10). Photolithographic resolution of 5 μm fingers was more readily achieved for IDAs due to the flat surface of the SiO_2. However, the yield of the IDAs was only about 20 %. Defects occurred from small pits in the silicon surface which were the result of anisotropic etching. In other cases portions of the carbon films did not adhere to the substrate, leaving holes in the arrays. About 75 % of the IDA samples had the two electrodes shorted together after fabrication, which was not always evident from visual inspection. A possible solution to the shorting problem would be reducing the width where the two electrodes overlap (500 μm in this work), reducing the area available for shorting.

The IDA samples were also resistant to anodic bonding, similar to the band electrodes, such that only 10 % of the samples bonded. Since Au samples were not as difficult to bond this possibly indicates a residue or contaminant left on the SiO_2 surface after reactive ion etching. When anodic bonding was successful, carbon was destroyed along the length of the flow channel covering the IDA. This could possibly be attributed to a high temperature or voltage drop across the flow channel between the Pyrex and the SiO_2. As a result of low construction yield, sample shorting, and destruction during anodic bonding, few IDA samples were tested. A CV of one electrode of a carbon IDA is

shown in Figure 3-13. Although this CV demonstrates that electrodes which survive the fabrication procedures are electrochemically active, the low yield prevented investigation of amperometry or recycling behavior of IDA samples. To improve construction yield, more stable carbon films are necessary, either through optimization of pyrolysis and etching procedures, or by investigation of other carbon deposition techniques. Also, at this time low temperature bonding methods are not available to replace anodic bonding. Further construction and characterization of dual carbon electrodes await development of these procedures.

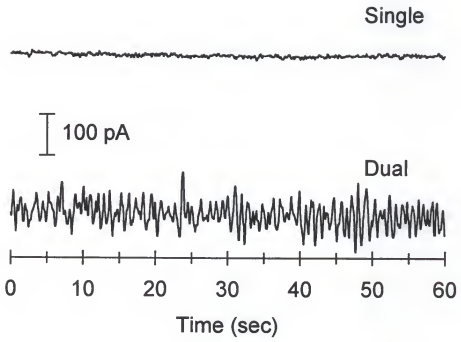

Figure 3-1. Comparison of noise levels between single and dual electrode mode for the Au parallel opposed recycling electrochemical detector.

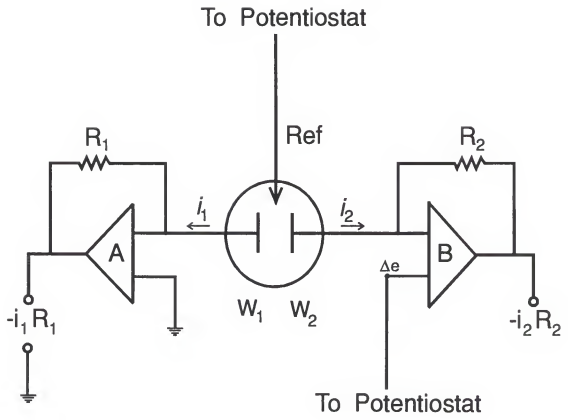

Figure 3-2. Abbreviated schematic of a bipotentiostat with parallel opposed electrodes W_1 and W_2. A and B are the current to voltage converters for W_1 and W_2 respectively, and R_1 and R_2 are feedback resistors. The thin layer of solution between the two parallel opposed electrodes results in a small resistance; noise currents which flow between the electrodes can be subsequently amplified by the current to voltage converters.

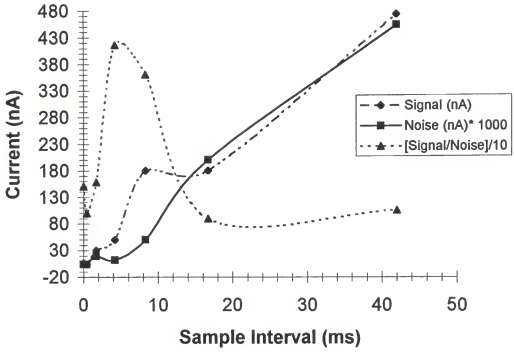

Figure 3-3. Signal and noise values for a typical single electrode detector at different sampling intervals. Note the scaling of the data as indicated in the legend. Measurements were made for injections of 10 μM $Fe(CN)_6^{4-}$ at a duty cycle of 0.02. The points at 0 ms sampling interval indicate measurements made with the EI-400 (no switching). Flow rate 440 nL/min.

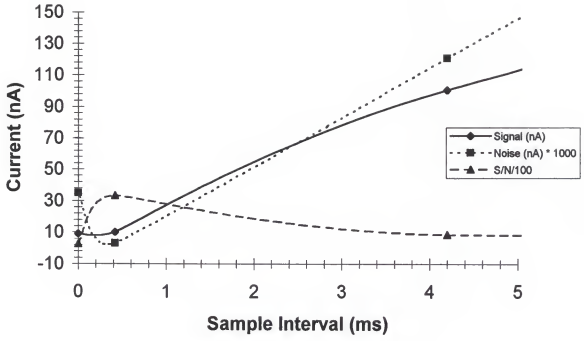

Figure 3-4. Signal and noise values for a detector in dual electrode (recycling) mode at different sampling intervals. Note the scaling of the data as indicated in the legend. Signal and noise measurements were made for injections of 10 μM $Fe(CN)_6^{4-}$ at a duty cycle of 0.5. The points at 0 ms sampling interval indicate measurements made with the EI-400 (no switching). Flow rate 320 nL/min.

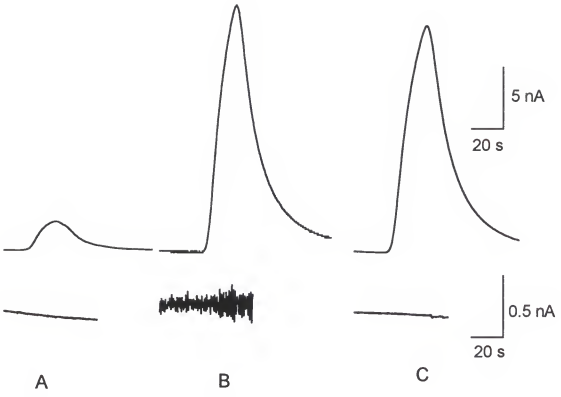

Figure 3-5. FIA current time traces for injections of 10 μM $Fe(CN)_6^{4-}$. A. Response of a single electrode measured with the EI-400 (no switching). B. Response of the same detector in dual electrode mode with no switching. C. Response with EI-401 at a sampling rate of 417 μs and a duty cycle of 0.02.

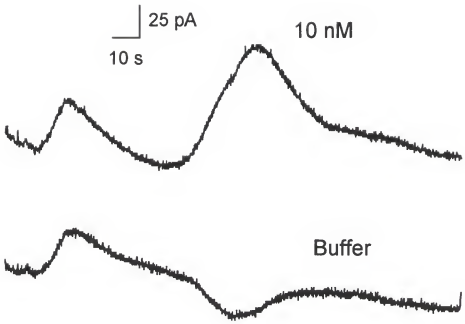

Figure 3-6. Current response for injection of 10 nM $Fe(CN)_6^{4-}$ with dual electrode detection at a 417 μs sampling interval. The current trace below is for a buffer injection. The small peaks at the start of the traces are system peaks caused by the injection.

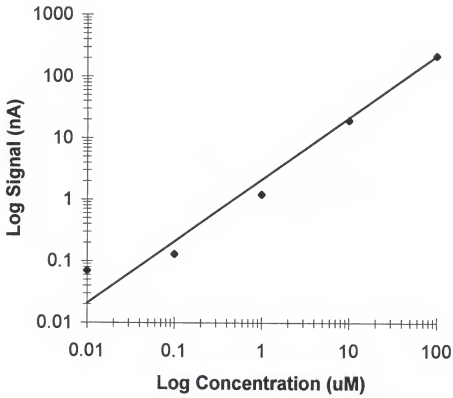

Figure 3-7. Log-log calibration plot for injections of $Fe(CN)_6^{4-}$ detected in dual electrode mode with a switching sample interval of 417 μs and a duty cycle of 0.02. The points are experimental data while the line is a best fit linear regression; correlation coefficient 0.99987.

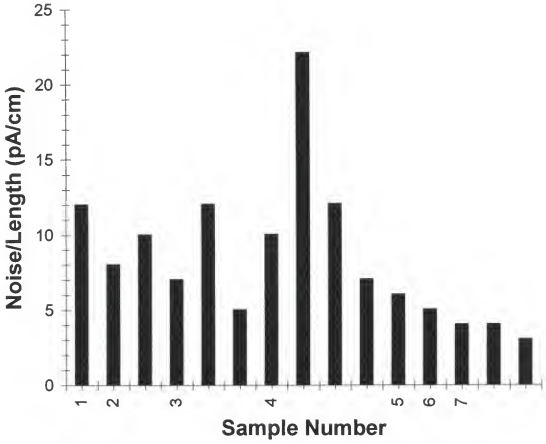

Figure 3-8. Noise/length ratio for single electrode detectors. Samples 1-4 are solid electrodes, while samples 5-7 are arrays with 10 μm fingers and 5 μm gaps. Multiple bars for a sample indicate data taken at different flow rates.

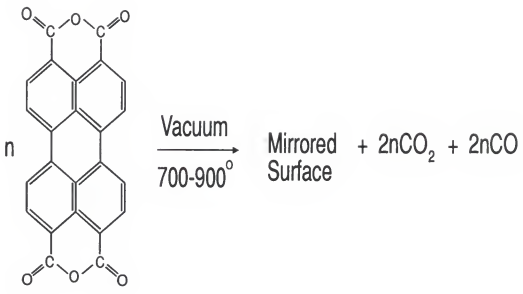

adapted from (60) Kaplan, M.L, Schmidt, P.H., Chen, C., and Walsh Jr., W.M. *Appl. Phys. Lett.* **1980**, 36(10), 867.

Figure 3-9. Pyrolysis reaction of 3,4,9,10-perylenetetracarboxylicdianhydride. Carbon films produced are mirrored. The mechanism of hydrogen loss is not known.

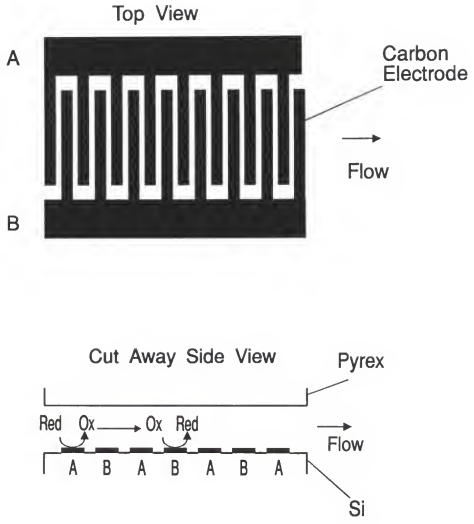

Figure 3-10. A carbon IDA configuration can also be used for recycling detection . The IDAs were fabricated on flat SiO_2 pieces, with flow channels etched into the Pyrex cover. Analyte molecules traveling through the detector cell will be recycled as they alternate between array fingers biased at the oxidation potential (A) and those biased at the reduction potential (B).

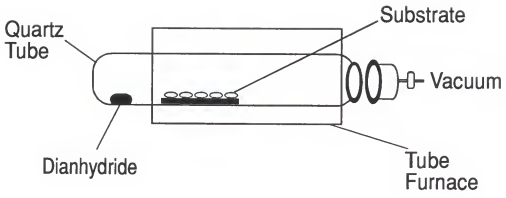

Figure 3-11. Schematic diagram of pyrolysis apparatus used to deposit carbon films. The quartz tube was 100 cm long by 2 inches in diameter, and the end was modified with a ball joint (size 75/50, 2 inch diameter). Samples were placed in the tube via this opening. Vacuum was applied by clamping a socket joint to the tube with a vacuum stopcock attached. The distance between the PDTA and the front of the samples was approximately 5 cm.

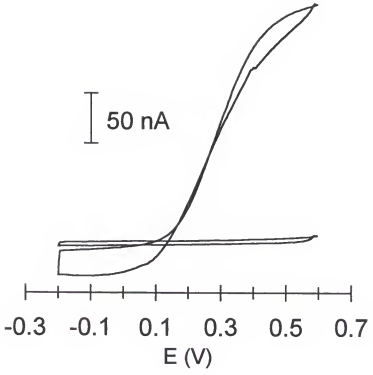

Figure 3-12. CV of chemical vapor deposited (CVD) carbon film electrode in 10 μM $Fe(CN)_6^{4-}$ (upper scan) and in buffer (0.1 M KH_2PO_4, lower scan). This CV is from a carbon band electrode with the same dimensions as the gold electrodes. Scan rate 50 mV/s.

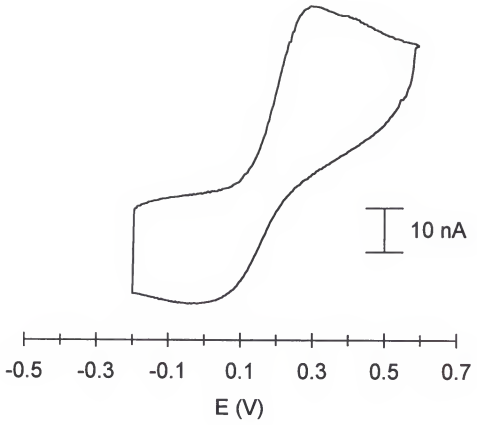

Figure 3-13. CV of single CVD carbon electrode of an IDA sample in 100 μM $Fe(CN)_6^{4-}$. Scan rate 50 mV/s.

CHAPTER 4
RANDOM WALK SIMULATIONS OF DIFFUSION IN RECYCLING AND EXOCYTOSIS DETECTION

Introduction

Digital simulation of electrochemical phenomena has been a useful tool in the prediction of concentration profiles and currents since its initial development in the late 60s (62). This chapter focuses on the use of random walk simulations to model the diffusion and detection of electroactive molecules at an electrode surface, both for the parallel opposed detector described in Chapter 2 and for exocytosis products of single cells detected at a microelectrode. Random walk simulations have been used to model the detection of catecholamines released from biological cells during exocytosis at a carbon fiber microelectrode (63), as well as diffusion between closely spaced band electrodes (64). The advantage of using this type of simulation is that it is well suited for probing different geometries of electrode configurations which can be investigated by simply adjusting the placement of the electrode(s) on a coordinate grid. This type of model allows a finite number of molecules to move in multiple directions along this grid, with one or more boundaries of the grid defined as the electrode surface. The Einstein equation describing diffusional motion can be used to calculate the time increment of each step in the walk depending on the diffusion coefficient of the analyte of interest:

$$(1) \qquad \sigma^2 = 2Dt$$

where σ is the diffusion distance, D is the diffusion coefficient in cm^2/s, and t is the time to diffuse the distance σ. A computer program is used to track molecules; when a molecule reaches a boundary defined as an electrode surface it can be either removed from the system or converted to the opposite redox state.

The first half of this chapter describes the simulation of molecular diffusion and subsequent electrochemical recycling in the parallel opposed detectors described in Chapter 2. Computer programs were written which allowed a given number of molecules to diffuse between two or more electrodes for a specific time and which kept track of the redox states and number of times each molecule was recycled when an electrode surface was reached. The simulations were developed to investigate different shapes, positions, and numbers of electrodes to determine which design would provide the most recycling of analyte molecules and therefore signal enhancement. The amount of recycling predicted for a certain detector design was compared to predictions for other geometries as a diagnostic comparison. The simulations were also used to predict effects of changing detector dimensions on the amount of recycling for each detector considered. The experimental amount of recycling obtained with parallel opposed detectors during FIA in Chapter 2 was compared to results of simulations under the same conditions. The simulations were helpful in predicting the amount of recycling and signal enhancement that should be expected during characterization of the flow through detectors.

The second half of this chapter describes three-dimensional random walk simulations designed to model the transport behavior of insulin and serotonin (5-HT) secreted from single pancreatic beta cells and then detected at an electrode surface

positioned near the cell surface. Amperometry at microelectrodes has been used in this and other laboratories to monitor secretion from single cells at the level of single exocytosis events (65,66). Figure 4-1 shows a depiction of exocytosis and the detection scheme used by coworkers in this laboratory to measure insulin and other compounds from single cells. A modified electrode was developed in this laboratory to detect exocytosis of insulin with high temporal resolution (67,68,69). 5-HT, which is secreted from the same vesicles as insulin, was also detected using a bare carbon fiber electrode to determine its usefulness as a marker of insulin. When glucose, tolbutamide, or muscarine were applied to β-cells, a series of current spikes corresponding to detection of exocytosis events were obtained when detecting insulin, 5-HT, or both compounds. Exocytosis detected with amperometry at a microelectrode results in multiple current spikes, each representative of a single exocytosis event. The shape of current spikes were different for the two substances with the width at half maximum (FWHM) height smaller for 5-HT. The difference in shape was attributed to the differences in storage and expulsion from the vesicles for the two compounds.

In this work, a three-dimensional random walk was developed to simulate the expected shape of current spikes resulting from measurement of these compounds. This was done to investigate the shapes of actual insulin and 5-HT current spikes, obtained by Mr. Craig Aspinwall, to determine differences in their methods of transport to the electrode (70). The model predicts shapes based on diffusion only; deviation of the shape of experimental spikes from the simulated ones indicates that other factors, such as dissolution, controlling the shape or width of current spikes.

Simulation of Recycling Electrochemical Detection

Experimental. A two-dimensional random walk was used to model diffusion and subsequent detection of electroactive molecules between two or more electrodes. The simulations were used to aid in the design of electrochemical cells and placement of electrodes within the cells. The objective was to determine dimensions of channel and electrode(s) which would give the maximum number of recycles, signal enhancement, and S/N ratio increase. Different geometries simulated as possible detectors are shown in Figure 4-2. For the simulations, the physical dimensions of the cell and electrode were variable, as well as the diffusion coefficient (D) of the analyte, the flow rate, and the number of analyte molecules. For each simulation, 1,000 molecules were allowed to diffuse within the cell for a residence time determined by dividing the volume of the detector by the flow rate specified. For each step of the random walk, the molecules moved one step in both the x- and y-dimensions (Figure 4-3). The x direction was defined as toward side walls of the channel (parallel to the electrodes), while the y direction was defined as toward the top or bottom of the channel (parallel to the side walls).

The Einstein equation and diffusion coefficient of an analyte were used to define the rate of diffusion. The direction of the move for each dimension was determined by a random number generator. Molecules that contacted coordinates defined as the electrode surface were converted to reduced or oxidized form as appropriate. The programs tracked the redox state, position, and number of oxidations and reductions for each molecule. In most cases, 10 simulations were performed and their results averaged. In cases where current was estimated from simulations, the charge passed was estimated by

multiplying the average number of times a molecule was oxidized, the number of molecules in the cell for a given concentration, and the charge of an electron. One electron transferred per oxidation was assumed for this system. Charge was divided by residence time in the cell to estimate the current expected for a given concentration and flow rate.

Results and discussion. As described in Chapter 2, the parallel opposed configuration was the primary detector investigated due to the simplicity of the design and the possible signal enhancement predicted. Figure 4-3 indicates the cell boundaries and parameters used in the simulation as well as a possible path for a molecule during simulation. Results of simulations performed specifying a 5 mm channel (electrode) length and a flow rate of 10 nL/min are shown in Table 4-1. The calculated current to electrode area ratio was used as a relative measure of S/N ratio. A copy of the source code for the parallel-opposed simulation program in Basic (RECYCL6C.BAS) is provided in Appendix B.

When considering the parallel opposed geometry, it is apparent that decreasing the gap between electrodes will decrease the time required to diffuse between the electrodes and therefore increase recycling (signal). However, if the cell and electrode width and length are kept the same as the gap is decreased (Table 4-1 A) then the volume of the cell will decrease which will decrease residence time in the cell and the amount of recycling possible. An alternative is to maintain the same cell volume as the gap size is decreased by increasing the width or length of the channel and electrodes (Table 4-1 B). In this case, the noise, which is nominally proportional to electrode area, will increase as the signal

from recycling is increased. As seen in the table, decreasing the gap while maintaining the maximum electrode area results in the greatest ratio of current to electrode area (assumed to be proportional to S/N); however, the increases are not as great as might be expected based strictly on consideration of how rapidly the molecules can diffuse between the electrodes. This is due to the decrease in volume as the gap is reduced. Alternatively, for a fixed cell volume of 0.25 nL, Table 4-1 shows that decreasing the electrode gap from 20 μm to 1 μm results in a signal enhancement of ~545-fold, but with the increase in electrode area, the current per electrode area only increases ~26-fold. The extremely high conversion efficiencies suggest that even with the increases in noise associated with this type of system, recycling electrochemical cells are capable of improvements in detection limits over single electrode detectors for microcolumn separations.

These results, as well as other simulations performed, provided estimates of signal and S/N increases (over single electrode detection) to be expected for detector cells developed in this work. The simulation results in Table 4-1 indicate that the best recycling would be observed with a detector which had a 1 μm separation between the two electrodes. However, this size flow channel would be most prone to clogging and also shorting of electrodes. Initially, cells with a 10 μm distance between the two electrodes were tested, for which conversion efficiencies were predicted to be 81-fold greater than a single electrode at a flow rate of 10 nL/min. In Chapter 2 a 22-fold increase was acheived at a flow rate of 37 nL/min while random walk simulations predicted a 16-fold increase. After characterization of cells with a 10 μm electrode distance, a 5 μm distance was used to further increase the recycling and signal enhancement. In Chapter 2, a 60-fold increase

in signal was observed with a 5 μm distance between electrodes. Electrochemical cells with channel depths of 3 μm were also fabricated to further increase signal enhancement. However, most of these channels were blocked initially or clogged soon after introduction of buffer solution. For this reason, a 5 μm channel depth was chosen for the remainder of experiments performed in this work (Chapter 3).

Random walk simulations were used not only to investigate possible designs of electrochemical detectors; they also served as predictions for how much recycling enhancement could be expected from microfabricated detectors which were tested with FIA. As stated in Chapter 2, the signal enhancement observed for the dual electrode parallel opposed detectors compared to the single electrode cells was dependent on the residence time of the analyte in the flow cell, or the flow rate. A cell which showed recycling with chronoamperometry was tested with FIA by repetitive injections of the same concentration of analyte at different flow rates, and the signal enhancement calculated for each one. The random walk simulation was performed for each flow rate investigated and the two sets of data compared (Figure 4-4). The good agreement (within 10 % at flow rates below 500 nL/min) of the random-walk simulations with experimental results suggests that the model may be used to predict the most fruitful approach to gain further enhancements in S/N ratios.

Side by side electrode geometry. Electrochemical flow cells with other electrode geometries were also considered and their performance simulated. A flow cell with the detection and recycling electrodes positioned side by side on one plane of the flow cell was simulated (RECYCLE7.BAS) (Figure 4-2 A). The results, averages of 10 simulations

at a flow rate of 10 nL/min (Table 4-2), are compared to those for a parallel opposed detector of similar dimensions. The conversion efficiencies predicted for side by side cells with similar electrode area and volume were significantly less than those predicted for the parallel opposed geometry. This can be attributed to the fact that unless a molecule is on the inside edge of an electrode (directly next to the gap), then it must diffuse further than just the distance (or gap) between the two electrodes to be recycled (Figure 4-2). In the parallel opposed case the diffusion distance required for recycling is defined by the depth of the channel in the flow cell. Side by side flow cells were not actually fabricated; simulation of this geometry was done to confirm that the model performed as we expected (larger conversion efficiencies for the parallel opposed case).

Four electrode configuration. Also investigated was an electrochemical cell with four electrodes (Figure 4-2 C), one detection electrode with a recycling electrode on either side (all in the flow channel), and a wide recycling electrode parallel opposed on the glass (RECYCLE8.BAS). For these simulations, the width of the channel was fixed at 50 μm and the length at 5 mm. (Table 4-3). This configuration gave 2-3-fold better S/N than the parallel opposed detector (Table 4-1 A) due to the larger recycling area and smaller detection electrode area (lower noise). Changing the gap between the detector and recycling electrodes did not significantly alter the results (Table 4-3 B). Also, increasing the detection electrode size from 5 to 10 μm wide resulted in increased recycling (signal) but a decrease in S/N ratio compared to the 5 μm cases (Table 4-3 C). This detector design was not fabricated; at the time reproducible definition of multiple electrodes of small dimensions in the flow channel was not feasible. This was due to the varying

thickness of the photoresist when spun over channels of 5-10 μm depth, as described in Chapter 2. However, a future possibility would be to fabricate the large recycling electrode in the channel and define the other three electrodes on the Pyrex surface.

Carbon fiber detection with recycling channel. High conversion efficiencies of carbon fibers when used as on column detectors in microcolumn LC made them candidates for use with electrochemical recycling. Simulations were developed to determine how much electrochemical recycling could improve their performance. The design consisted of a carbon fiber detector electrode inserted into the end of a microfabricated flow channel which has all four walls defined as a recycling electrode (Figure 4-3 D). This configuration is similar to regular on-column detection in microcolumn LC where a carbon fiber is inserted into the end of a capillary column with the exception of the recycling walls and the square shape of the flow channel.

The results for these simulations are shown in Table 4-4. Results for parallel opposed detectors of similar detector area and volume are also shown. The channel dimensions were adjusted until the volume, area, and residence times were similar to the parallel opposed case so a direct comparison could be made. Current was calculated in the same manner as described earlier for the parallel opposed configuration. The simulation results indicate that this type of detector could exhibit much greater S/N enhancements than the parallel opposed detector; a maximum of a 34-fold enhancement over the parallel opposed case was predicted for a 0.5 mm carbon fiber inserted into a channel with approximately 25 μm walls.

Microfabricated channels with four recycling walls were fabricated. However, even with the aid of a micromanipulator it was very difficult to insert a carbon fiber into channels of such small dimensions. This was due to the opaqueness of the silicon portion of the detector. It could not be illuminated well enough to allow insertion of the fiber, in contrast to the transparent fused silica capillaries used in microcolumn LC. A shop microscope and bulb provide enough light to image the inner diameter of a capillary; this was not the case for the silicon microfabricated detectors. Therefore these cells with four recycling walls and a carbon fiber detector electrode could not be tested to compare their actual recycling capabilities to the simulations. Future possibilities would be to fabricate this detector using all Pyrex (which would require bonding of two Pyrex pieces), or to use a fused silica capillary modified to have a portion of its inner diameter metallized.

Microelectrode array simulations. One method of reducing noise and increasing S/N ratios in ECD is to use an electrode array. Theoretical and practical aspects of arrays have been the subject of much investigation by several groups (52). The overlap of the diffusion layers of the array fingers maintains much of the signal of the solid electrode; nonlinear diffusion to the electrode edges results in increased mass transport of electroactive material to the surface (56). At the same time, the noise level is reduced due to the smaller electrode area of the array, resulting in an overall increase in the S/N ratio (Figure 4-3 E). Electrochemical array detectors fabricated with similar dimensions should exhibit increased S/N levels over solid parallel opposed detectors.

Random walk simulations were written (RECYCL11.BAS) before the fabrication of array detectors to estimate the magnitude of recycling and S/N enhancement possible

with this design compared to solid parallel opposed electrodes. To fabricate a detector with the greatest S/N increase relative to the solid electrode, a simulation program was designed which allowed variation of the array finger size, gap width between fingers, and number of array fingers as well as the parameters present in previously described simulations. Resolution of the lithography equipment limited structures to about 5 μm dimensions, although a 1 μm or less finger width and gap are possible . Due to this limitation, 5 μm was used as the finger width for simulations, and the gap width between fingers was varied. The number of oxidations was used as a relative measure of signal in this case, with the electrode area as a relative measure of noise.

The resulting simulated signal, noise, and S/N ratios for 5 μm finger arrays are plotted in Figure 4-5. The points at 0 μm gap distance represent the simulation for a solid electrode. The simulated signal decreased somewhat as a function of increasing gap width as shown in Figure 4-5 A, due to the smaller active electrode area. For the same reason, the noise decreased with an increase in gap width as shown in Figure 4-5 B. With increasing gap width the number of fingers, and therefore the area, decreased. The combined effects on S/N ratios is shown in Figure 4-5 C. Compared with solid parallel electrodes, the S/N of an array with 5 μm wide fingers increased with an increase in gap size up to a gap of approximately 5 μm, where the S/N ratio leveled off. At values above 8 μm, the S/N began to decrease, with a maximum S/N improvement of approximately 2-fold. These results prompted fabrication of electrochemical cells with array detectors of 5

μm fingers with 5 and 10 μm gaps between them; their results were described in Chapter 3.

Results and discussion. The development of simulation programs for different recycling electrode geometries was straightforward and the programs simple to execute. Simulation of different electrode configurations was helpful in determining if recycling enhancement would be comparable to the parallel opposed case and if the detector should be fabricated. Of the designs simulated, only the side by side geometry did not show improved performance over the parallel opposed configuration. The four electrode and array designs showed 3-fold and 2-fold increases, respectively, of predicted S/N ratios over the parallel opposed case. However, difficulties in definition of electrodes smaller than 5 μm (or even of 5 μm in a flow channel) made fabrication of these detectors impractical. Improvements in the definition of smaller electrodes could make these designs feasible as sensitive detectors. In Chapter 3, an LOD of 20 nM was observed in one case for an array detector, an improvement over the 50 nM LOD observed with the parallel opposed cells. The carbon fiber inserted into a recycling channel predicted the largest S/N improvement over the parallel opposed case (up to 34-fold). Therefore, development of fabrication procedures for an all Pyrex channel or metallized capillary could be a beneficial experiment in the future.

Despite the improved performance predicted for detectors of other geometries, the advantage of parallel opposed detectors was the relative ease of construction coupled with significant recycling and enhancement of signal. For the testing of parallel opposed detectors, the simulations were informative by providing an estimate of signal

enhancement possible over single electrode detection. It was also observed that the enhancement predicted by the model agreed fairly well with experimental values at flow rates in the range of those used for microcolumn separations. For example, for the data shown in Figure 4-4, the amount of simulated signal enhancement deviated from the experimental data by an average of 10 % at flow rates below 500 nL/min. In the future, simulations could be extended to other recycling geometries considered for fabrication. Also, flow could be incorporated into the model to more closely simulate conditions present during testing of parallel opposed detectors.

Simulation of Insulin and Serotonin Exocytosis Spike Shapes

The focus of this project was to investigate through simulation the mechanism of insulin and 5-HT release from single pancreatic beta cells when stimulated chemically. Due to the shapes and widths of the current-time traces obtained experimentally by Mr. Craig Aspinwall for these compounds, it was postulated that 5-HT release is controlled by diffusion, while insulin release is also controlled by other factors such as dissolution (69). To confirm the experimental results, transport of insulin and 5-HT from the vesicle to the electrode and subsequent detection were simulated with a diffusion-based three-dimensional random walk simulation.

Experimental. A diagram of the model geometry used in these simulations is shown in Figure 4-6. Electrode area was calculated for an elliptical surface. The cell was considered a hemisphere with a radius of 5 μm with the electrode positioned directly over the apex of the cell with a 1 μm gap between the electrode and cell. These values as well as cell and electrode dimensions could be varied during simulations; values given here

were selected to closely resemble experimental conditions used. Figure 4-6 illustrates exocytotic release from different points on the cell surface.

An exocytosis event was represented by a point source of 5,000 molecules diffusing from a location on the cell to the electrode. Events originating at the apex of the cell travel the shortest distance to the electrodes, while events originating at the base of the cell require molecules to travel a maximum distance to the electrode surface (Figure 4-6). The time increment per step was calculated from the Einstein equation as described earlier for parallel opposed detectors. Step size was calculated as one tenth of the diffusion distance from the cell to the electrode, and step direction was determined by a random number generator. Molecules reaching the electrode surface were detected and removed from the system. Those reaching insulation surrounding the carbon fiber were deflected to their previous position. Simulations were allowed to continue for 3000 steps; increasing this number did not affect the results. For the simulations, insulin was considered to have a diffusion coefficient of 2.0×10^{-6} cm^2/s and 5-HT 6.0×10^{-6} cm^2/s as described previously (66). The number of electrons reaching the electrode for each step of the walk were divided by the time increment per step and plotted as a function of time.

To reduce noise caused by the finite number of particles used for simulations, a Savitsky-Golay smoothing algorithm was used on the resulting data. The smoothing and also the measurement of the maximum response and FWHM were done with a Labwindows data analysis program written in house. Each spike simulated was the result of 5000 particles released; 10 simulations were averaged for each set of conditions tested. To compare experimentally obtained spike shapes with simulated data, selected simulated

spikes were normalized to the experimental half width in milliseconds (ms) and the maximum response in picoamps (pA). Normalization consisted of first multiplying all the time increments by the ratio of the experimentally obtained half width to that of the simulated peak. The simulated response was normalized by multiplying all values by the ratio of the experimental current response to that of the simulated spikes.

Results and discussion. Figure 4-7 shows examples of simulated spikes for insulin which were smoothed but not normalized, showing the effects of distance (Figure 4-7 A) and diffusion coefficient (Figure 4-7 B) on the spike width and height. The expected width for an experimental spike depends on the distance between the electrode and the site of release, which depends on where the exocytosis event occurs on the cell. Since the site of release is not known, the model cannot be used to fit directly to a specific spike. However, it is possible to predict the limits of spike widths based on the model. The half widths of simulated insulin spikes (1.5 ms) were on the average three times as wide as the half widths for 5-HT (0.5 ms) if the molecules were allowed to freely diffuse out of the exocytosis sites from a site immediately next to the electrode. The difference in widths is due to the difference in diffusion coefficients as shown in Figure 4-7 B. If exocytosis occurred 2.5 μm away from the top of the hemispherical cell (Figure 4-6), the predicted widths were 21 ms for insulin and 7.4 ms for 5-HT. Experimentally, Mr. Aspinwall observed that 13 % of the 5-HT spikes and 67 % of the insulin spikes were over their predicted width at this distance. If an exocytosis event occurred at the base of a cell (Figure 4-6), the furthermost possible point from the electrode, the predicted width was 58 ms for insulin and 22 ms for 5-HT. Experimentally, none of the 5-HT spikes but 22 %

of the insulin spikes were over the widest expected widths based on diffusion. Overall, the average half widths obtained experimentally for insulin were approximately 10 times the width as 5-HT spikes (37 ms for insulin and 3.6 ms for 5-HT). This result is in contrast to the 3-fold difference based solely on the diffusion model. A significant fraction (22 %) of the insulin spikes were wider than predicted even for release at the furthest point from the electrode. These data support the idea that other factors were influencing the width of the insulin current spikes besides diffusion.

The unknown release site of exocytosis on the cell limits the comparison of modeled spikes to specific experimental ones, as stated earlier. However, previous studies of adrenaline secretion from adrenal chromaffin cells showed that if simulated spikes were normalized to the peak height and width at half height of a measured spike, then the general shape predicted by the model can be compared to the measured spike (62). Insulin and 5-HT spikes which have undergone this manipulation are shown in Figure 4-8. When normalized for peak height and width, the shape of the insulin spikes are approximately what would be expected by diffusion. However the difference in the half widths of experimental insulin spikes from simulated values indicates that this is not the only factor influencing the widths. The difference in the shape and width of the 5-HT and insulin spikes is best attributed to differences in the storage of the two compounds (71). Insulin is stored as a complex with Zn^{2+} in a solid form. The state of 5-HT is not known but is postulated to be in solution or loosely bound to vesicular proteins (69). Thus, 5-HT escapes more readily from a vesicle during exocytosis, resulting in spike widths that are within the limits expected for diffusion. The dissolution and dissociation of insulin from

Zn^{2+} results in slower dynamics of release and therefore broader spikes than those predicted by the diffusion based model.

The random walk simulations provided valuable contributions in the assessment of current response shapes obtained for insulin and 5-HT at a microelectrode. Further investigations are possible with random walk models. The kinetics of the dissolution and dissociation of insulin from Zn^{2+} could be incorporated into the model to further confirm that these processes are what are affecting the experimental spike shape. Also, detection of compounds which undergo a following reaction or are recycled after detection could be simulated. In addition, the random walk model could be modified such that the exocytosis release site could be determined by a random number generator. This type of model could also be applied to cell measurement experiments where two or more micron sized electrodes are used to measure exocytosis at specific sites on the cell.

Table 4-1. Effect of Parallel Opposed Cell Geometry on Performance: Simulation Results*

	Channel Depth (μm)	Electrode Width (μm)‡	Electrode Area ($cm^2 \times 10^3$)	Detector Volume (nL)	Residence Time (s)	Conversion Efficiency (%)	Current (nA)~	Current/ Electrode Area ($nA/cm^2 \times 10^{-3}$)†
A	1.0	50	2.50	0.25	1.5	68,000	1092	437
	2.0	50	2.50	0.50	3.0	33,900	546	218
	5.0	50	2.50	1.30	7.5	16,400	274	109
	10	50	2.50	2.50	15	8,100	131	52
	20	50	2.50	5.00	30	4,000	64	25
B	1.0	50	2.50	0.25	1.5	68,000	1091	436
	2.0	25	1.30	0.25	1.5	16,900	272	217
	5.0	10	0.50	0.25	1.5	3,200	52	103
	10	5.0	0.25	0.25	1.5	700	12	48
	20	2.5	0.13	0.25	1.5	100	2	17

* For all simulations, channel length was 5 mm, analyte concentration was 100 μM, flow rate was 10 nL/min, diffusion coefficient was 6×10^{-6} cm^2/s, and 1-electron was transferred per oxidation

~ Calculated as described in the Experimental section

† Used as a relative S/N

‡ Channel width was the same as the electrode width

Table 4-2: Results of Random Walk Simulations: Parallel Opposed vs.Side by Side

Channel Width (μm)	Channel Depth (μm)	Channel Length (mm)	Channel Vol. (nL)	Electrode Area ($cm^2 \times 10^3$)	Gap Width (μm)	Conversion Efficiency (%)
A. Parallel Opposed Electrode Configuration						
20	5.0	5.0	0.5	1.0	--	6400
20	10	5.0	1.0	1.0	--	3400
20	10	2.5	1.0	0.5	--	1700
50	5.0	5.0	1.3	2.5	--	16000
50	10	5.0	2.5	2.5	--	8500
B. Side by Side Electrode Configuration*						
45	5.0	5.0	0.6	1.0	5.0	500
45	5.0	5.0	1.1	1.0	5.0	1000
45	10	2.5	1.0	0.5	5.0	600
105	10	5.0	1.3	2.5	5.0	700
105	10	50	2.5	2.5	10	1000

*Detection electrode width the same as part A.

Table 4-3. Simulation Results for a Four Electrode Recycling Electrochemical Cell*

	Channel Depth (μm)	Detection Electrode Width (μm)	Detection Electrode Area ($cm^2 \times 10^{-3}$)	Gap Width (μm)	Recycling Electrode Width (μm, each)	Channel Volume (nL)	Conversion Efficiency (%)	Current (nA)	Current/ Electrode Area ($nA/cm^2 \times 10^{-3}$)
A	1.0	5.0	0.25	5.0	15	0.25	9300	150	600
	5.0	5.0	0.25	5.0	15	1.3	3500	56	220
	10	5.0	0.25	5.0	15	2.5	2600	42	170
B	1.0	5.0	0.25	10	10	0.25	9800	158	632
	5.0	5.0	0.25	10	10	1.25	3500	56	220
	10	5.0	0.25	10	10	0.25	2500	40	160
C	1.0	10	0.5	10	10	0.25	16000	257	514
	5.0	10	0.5	10	10	1.25	5000	80	160
	10	10	0.5	10	10	2.5	3400	55	110

*Residence times were 15, 7.5, and 1.5 sec for channel depths of 10, 5, and 1 μm, respectively.
Flow rate 10 nL/min.
Channel Width 50 μm, Length 5 mm

Table 4-4. Simulation Data for Carbon Fiber Inserted Into a Recycling Flow Channel

Detector Electrode Length (mm)	Electrode Area ($cm^2 \times 10^{-3}$)	Channel Depth (μm)	Channel Width (μm)	Channel Volume (nL)	Conversion Efficiency (%)	Current (nA)	Current/ Electrode Area ($nA/cm^2 \times 10^{-3}$)
A. Parallel Opposed Electrode Configuration							
10	50	5.0	50	0.25	3,200	52	103
5.0	0.25	10	50	0.25	700	12	48
2.5	0.13	20	50	0.25	100	2	17
B. Carbon Fiber Recycling Configuration							
2.0	0.63	14	14	0.25	15000	241	383
1.0	0.31	18	18	0.25	9200	148	477
0.5	0.16	24	24	0.25	5900	95	593

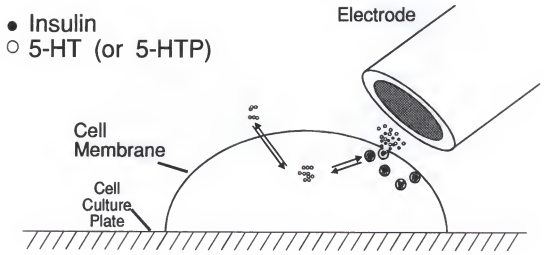

Figure 4-1. Schematic diagram of cell exocytosis and detection with a micron sized electrode. Exocytosis occurs when small packets of chemicals called vesicles fuse with the cell membrane. The contents of the vesicle are then released to the extracellular fluid, where electroactive species can be detected at the electrode surface.

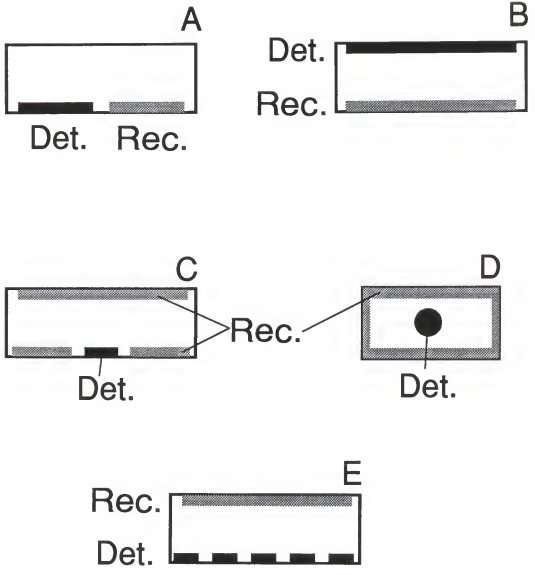

Figure 4-2. Schematic diagrams of different electrode configurations which were simulated with a two-dimensional random walk. Dimensions and conditions are given in the text. The electrode specified as the detection electrode(s) is represented by "Det", while "Rec" represents the electrode defined as recycling. A. Side by side electrode configuration B. Parallel opposed configuration as described in Chapter 2. C. Four electrode configuration. D. Carbon fiber detection with a recycling channel. E. A version of the parallel opposed configuration where the detection electrode is an array as opposed to a solid electrode. Note the of the electrode thickness' are shown larger for clarification (not shown to scale).

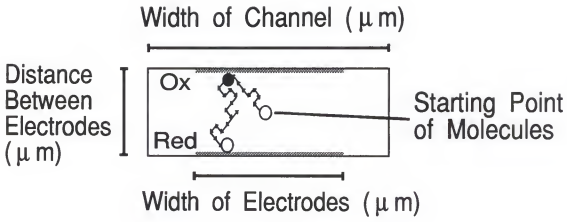

Figure 4-3. Schematic of two-dimensional random walk model for the parallel opposed electrode configuration. Open circles represent the reduced form of a model molecule while the solid circle represents the oxidized form. Molecules were allowed to move randomly in the x and y directions, and the number of oxidations and reductions for each molecule tallied. The simulation model could be changed by varying the parameters shown as well as the length of the channel, flow rate, number of molecules, and the number of simulations to be performed for each set of conditions.

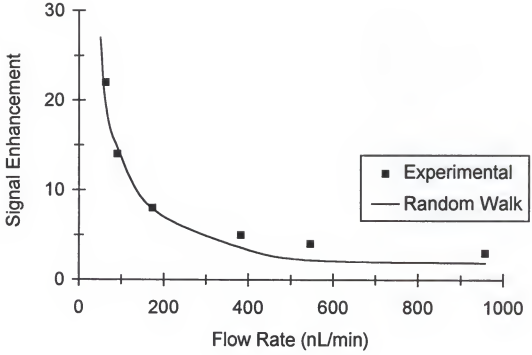

Figure 4-4. Plot of signal enhancement as a function of flow rate for a dual electrode detector during FIA. The solid line indicates values predicted with the random walk simulation, while the solid squares indicate experimental values. Signal enhancement was calculated as described in the text. Samples and conditions were the same as those indicated in Figure 2-13.

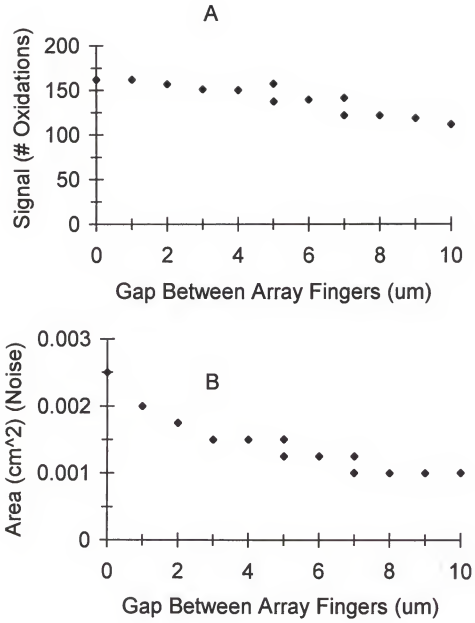

Figure 4-5. Simulation results for a 5 μm width finger array with varying gap size between fingers. The total width of the channel was approximately 50 μm, while the depth of the flow channel was 5 μm. The volume was approximately 1.25 nL at a flow rate of 10 nL/min. Each data point is the average of ten simulations. A. Number of oxidations plotted as a function of gap width. B. Area (relative to noise) plotted as a function of gap width.

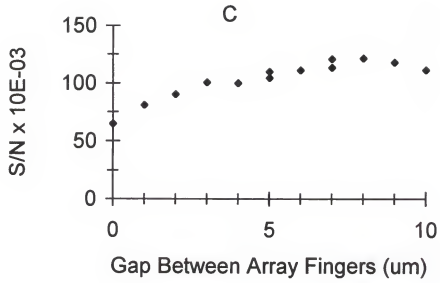

Figure 4-5 continued. C. S/N ratio plotted as a function of gap width for an array electrode. The ratio of the number of oxidations obtained in the simulation (A) to the electrode area (B) was used as relative S/N.

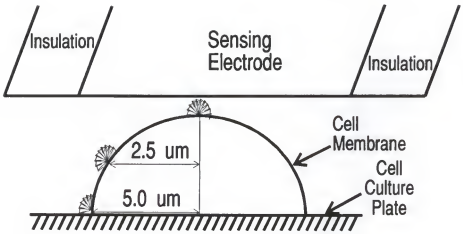

Figure 4-6. Illustration of three-dimensional random walk simulations. Molecules are defined as point sources on the surface of the hemisphere at the top, base, or other point on the cell surface as shown. The electrode surface is perpendicular to the plane of the paper, a cylinder-shaped electrode surrounded by insulation.

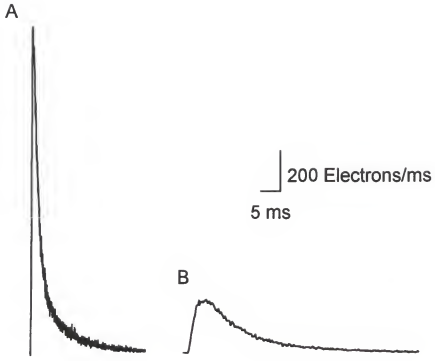

Figure 4-7 A. Simulated insulin spikes obtained from a three-dimensional random walk which have not been normalized. (A) The electrode to cell distance was 1 μm with D = 2.0×10^{-6} cm^2/s, resulting in a half width of 1.5 ms. (B) The electrode to cell distance was 2.5 μm with the same D as (A), resulting in a half width of 11 ms. The number of electrons detected per step was divided by the time per random walk step to calculate an estimated current. The spikes are the average of ten simulations of 5000 particles each which had been smoothed with a 5 point Savitsky-Golay filter.

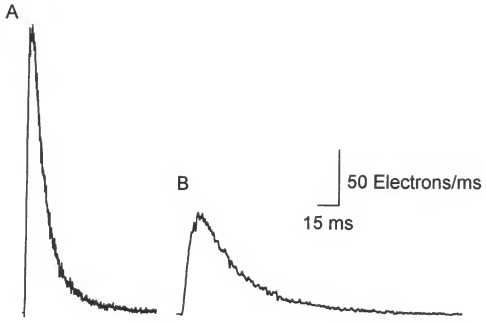

Figure 4-7 B. Simulated insulin spikes obtained from a three-dimensional random walk which have not been normalized. (A) Electrode to cell distance was 2.5 μm with $D = 2.0 \times 10^{-6}$ cm^2/s, resulting in a half width of 11 ms. (B) Simulation was done at the same electrode to cell distance as (A), with $D = 6.7 \times 10^{-7}$ cm^2/s. The half width for this spike was 30 ms. The number of electrons detected per step was divided by the time per random walk step to calculate an estimated current. The spikes are the average of ten simulations of 5000 particles each which had been smoothed with a 5 point Savitsky-Golay filter.

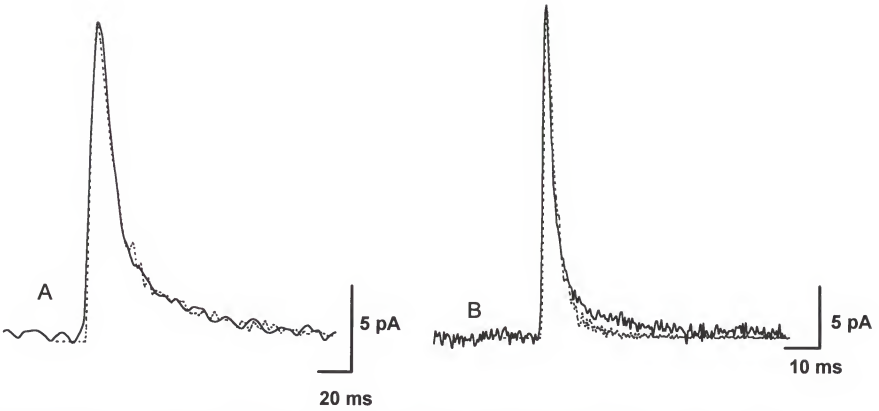

Figure 4-8. Comparison of current spike shapes for 5-HT and insulin. A. A spike for insulin detection and B) A spike for 5-HT. The dashed line is a simulated curve that is normalized to the height and width of the experimental peaks. The fluctuations in the simulated peaks are due to the small number of molecules used in the random walk.

CHAPTER 5
CONCLUSIONS AND FUTURE WORK

Microfabrication of single and dual electrode cells having volumes compatible with capillary LC and CZE was accomplished. Signal enhancements of over 60-fold were achieved in electrochemical cells at nL/min flow rates typical of capillary separation methods. Even with the noise increase which occurred during dual electrode mode, S/N improvements of 8-fold over a single electrode detector were possible. A 50 nM LOD was achieved for ferrocyanide. Although higher than carbon fiber detectors, this LOD was an initial indication of the utility of parallel opposed recycling detectors for capillary separations.

The EI-401 potentiostat switching system was constructed to reduce noise increases observed during recycling dual electrode detection. The combined effects of lowered noise levels and increased signal due to analyte recycling resulted in a S/N increase of 10-fold over single electrode detection at a sampling rate of 417 μs. This resulted in a 1-5 nM LOD for ferrocyanide, an improvement of at least 10-fold over results obtained without switching. The use of samples with 5 μm channel depths could improve the LOD even further. Coupling of these detectors to microcolumn separation systems in conjunction with the EI-401 is definitely a fruitful area for future work.

The noise level of single Au microfabricated electrodes was reduced by 2.5-fold through the construction of microelectrode arrays. Improvements in fabrication to

increase the yield of small (< 5 μm) dimension electrodes will allow further investigation of improvements in performance of recycling parallel opposed detectors.

The fabrication of carbon film electrodes was accomplished through the pyrolysis of PTDA at 900 °C. Although this method resulted in carbon films suitable for use as electrodes, limitations were encountered. Pyrolysis was not suitable for deposition on Pyrex due to the high temperature required. The development of a lower temperature carbon deposition method would facilitate the fabrication of parallel opposed detectors with carbon electrodes. One possibility would be to either sputter or evaporate directly a carbon source. A second alternative would be the decomposition of low molecular weight hydrocarbon gasses. A second limitation encountered was the decomposition of deposited carbon films during anodic bonding. Further investigation of carbon based electrodes will await improvements in fabrication procedures.

Prevalent throughout the projects presented here was the limitations presented by anodic bonding. While providing a good seal, anodic bonding was shown to oxidize and contaminate electrode surfaces, possibly increasing noise levels and decreasing the active electrode area. Development of a low temperature bonding method would be an important venture for future work in this project. One option would be the application of a spin-on or evaporated low melting temperature glass layer between the two pieces of the detector.

The utility of random walk simulations in electrochemical problems was demonstrated in this work. Simulation of recycling detectors allowed investigation of the performance of several possible designs. Modeling of parallel opposed detectors was used

to predict the amount of recycling possible for given cell dimensions and flow rates during FIA. The model deviated from experiment by 10 % at flow rates below 500 nL/min. In the future, effects of flow on recycling detection could be added to the simulation to closer resemble FIA conditions. Even without this addition, the programs are useful in investigation of possible detector geometries.

Three dimensional random walk simulations were used to investigate the shape of insulin and 5-HT peaks resulting from exocytosis products detection at a microelectrode. Experimental 5-HT current spikes were of similar half width values as simulated spikes (0.5 ms), while 22 % of experimental insulin spikes were wider than the values predicted by the model, even at the point on the cell furthermost from the electrode. The difference in the half widths of experimental insulin spikes from simulated values indicates that diffusion is not the only factor influencing the widths. In future work, more complex situations could be simulated with these methods. For example, simulations could be designed, by modification of the current programs, to include kinetic processes thought to contribute to the shape of the peaks.

The use of microfabrication has allowed construction of small volume electrochemical cells which have achieved higher signal enhancements than any published parallel opposed recycling detector. With the development of a batch fabrication method and low temperature deposition and bonding procedures, recycling electrochemical detectors could achieve detection limits in the low to sub attomole range.

REFERENCES

1. Ewing, A.G., Mesaros, J.M., and Gavin, P.F. *Anal. Chem.* **1994,** *66,* 527A.

2. Lunte, S.M., Lunte, C.E., and Kissinger, P.T. *Laboratory Techniques in Electroanalytical Chemistry,* 2nd ed., Marcel Dekker, Inc. New York, **1996** .

3. Warner, M. *Anal. Chem.* **1994,** *66,* 601A.

4. Stulik, K., and Pacakova, V. *Crit. Rev. Anal. Chem.* **1994,** *14,* 297.

5. Fleet, B., and Little, C. J. *J. Chromatogr. Sci.* **1974,** *12,* 747.

6. Roston, D.A., Shoup, R.E., and Kissinger, P.T. *Anal. Chem.* **1982,** *54,* 1417A.

7. Fenn, R.J., Siggia, S., and Curran, D.J. *Anal. Chem.* **1978**, *50,* 1067.

8. Purdy, W.C. and Weber, S.G. *Anal. Chem.* **1982,** *54,* 1757.

9. Ou, T., Moldoveanu, S., and Anderson, J.L. *J. Electroanal. Chem.* **1988,** *247,*1.

10. Radzik, D.M., and Lunte, S.M. *Crit. Rev. Anal. Chem.* **1989,** *20,* 317.

11. Kissinger, P.T., Bratin, K., King, W.P., and Rice, J.R. *ACS Symp. Ser.* **1980,** *136,* 57.

12. Allison, L.A., and Shoup, R.E. *Anal. Chem.* **1983,** *55,* 8.

13. Briner, R.C., and Bratin, K. *Current Separations.* **1980,** *2,* 1.

14. Kissinger, P.T., Bratin, K., Davis, G.C., and Pachla, L.A. *J. Chromatogr. Sci.* **1979,** *17,* 137.

15. MacCrehan, W.A., Durst, R.A., and Bellama, J.M. *Anal. Lett.* **1977,** *10,* 1175.

16. Allison, L.A., Mayer, G.S., and Shoup, R.E. *Anal. Chem.* **1984,** *56,*1089.

17. Karn, J.A. Mohabbat, T., Greenhagen, R.D., Decedue, C.J., and Lunte, S.M. *Current Separations.* **1992,** *11,* 57.

18. Chen, J., and Weber, S.G. *Anal. Chem.* **1995,** *67,* 3596.

19. Manz, A., and Simon, W. *J. Chromatogr. Sci.* **1983**, *21*, 326.

20. Knecht, L.A., Guthrie, E.J., and Jorgenson, J.W. *Anal.Chem.* **1984**, *56*, 479.

21. Olefirowicz, T.M. and Ewing, A.G. *Anal. Chem.* **1996,** *62*, 1872.

22. Cooper, B.R., Jankowski, J.A., Leszczyszyn, D.J., Wightman, R.M., and Jorgenson, J.W. *Anal. Chem.* **1992,** *64*, 691.

23. Kennedy, R.T., St. Claire, R.L. III, White, J.G., and Jorgenson, J.W. *Mikrochim. Acta.* **1987,** *2*, 37.

24. Oates, M.D., Cooper, B.R., and Jorgenson, J.W. *Anal. Chem.* **1990,** *62*, 1573.

25. Kovacs, G.T.A., Petersen, K. and Albin, M. *Anal. Chem.* **1996,** *68*, 407A.

26. Angell, J. B., Terry, S.C., and Barth, P.W. *Sci. Amer.* **1983**, *248*(4), 44.

27. Roylance, L.M., and Angell, J.B. *IEEE Trans. Electron. Devices.* **1979,** *ED-26*, 1911.

28. Petersen, K.E. *Proc. IEEE.* **1982,** *70*, 420.

29. Hornbeck, L.J. *Proc. SPIE.* **1990,** *1150*, 86.

30. Terry, S.C., Jerman, J.H. and Angell, J.B. *IEEE Trans. Electron. Devices.* **1979,** *ED-26*, 1880.

31. Kounty, L.B., Schmalzing, D., Taylor, T.A., and Fuchs, M. *Anal. Chem.* **1996,** *68*, 18.

32. Woolley, A.T., and Mathies, R.A. *Anal. Chem.* **1995,** *67*, 3676.

33. Woolley, A.T., Hadley, D., Landre, P., deMello, A.J., Mathies, R.A., and Northrup, M.A. *Anal. Chem.* **1996,** *68*, 4081.

34. von Heeren, F., Verpoorte, E., Manz, A., and Thormann, W. *Anal. Chem.* **1996,** *68*, 2044

35. Liang, Z., Chiem, N., Ocvirk, G., Tang, T., Fluri, K., and Harrison, D.J. *Anal. Chem.* **1996,** *68*, 1040.

36. Moore, Jr., A.W., Jacobson, S.C., and Ramsey, J.M. *Anal. Chem.* **1995,** *67*, 4184

37. Morita, M., Longmire, M.L., and Murray, R.W. *Anal. Chem.* **1988,** *60,* 2770.

38. Samuelsson, M., Armgarth, M., and Nylander, C. *Anal. Chem.* **1991,** *63,* 931.

39. Tatistcheff, H.B., Fritch-Faules, I. and Wrighton, M.S. *J. Phys. Chem.* **1993,** *97,* 2732.

40. Niwa, O., Xu, Y., Halsall, H.B., and Heineman, W.R. *Anal. Chem.* **1993,** *65,* 1559.

41. Meyer, H., Drewer, H., Grundig, B., Cammann, K., Kakerow, R., Manoli, Y. Mokwa, W., and Rospert, M. *Anal. Chem.* **1995,** *67,* 1164.

42. Niwa, O., Torimitsu, K., Morita, M., Osborne, P., and Yamamoto, K. *Anal. Chem.* **1996,** *68,* 1865.

43. Reay, R.J., Dadoo, R., Storment, C.W., Zare, R.N., and Kovacs, G.T.A. *Proc. of Solid State Sensor and Actuator Workshop. 1994,* Hilton Head, S.C. June 13-16, 61.

44. Slater, J.M.and Watt, E.J. *Analyst.* **1994,** *119,* 2303..

45. Gavin, P.F., and Ewing, A.G. *J. Am. Chem. Soc.* **1996,** *118,* 8932.

46. Kennedy, R.T. Ph.D. Dissertation, University of North Carolina Chapel Hill, **1988**.

47. Matsue, T., Aoki, A., Abe, T., and Uchida., I. *Chem. Lett.* **1989,** 134.

48. McClintock, S.A. and Purdy, W.C. *Anal. Chim. Acta.* **1984,** 166, 171.

49. Goto, M., Zou, G., and Ishii, D. *J. Chromatog.* **1983,** 268, 157.

50. Goto, M., Zou, G., and Ishii, D. *J. Chromatog.* **1983,** *275,* 271.

51. Wallis, G., and Pomerantz, D.I. *J. Appl. Phys.* **1969,** *40,* 3946.

52. Josowicz, M., Janata, J., and Levy, M. *J. Electrochem. Soc.* **1988,** *135,* 112.

53. Baginski, T.A., Jaeger, R.C., Fosdick, L.E., and Anderson, J.L. *Anal. Chem.* **1986,** *58,* 2750.

54. Weber, S.G., and Long, J.T. *Anal. Chem.* **1988,** *60,* 903A.

55. Morgan, D. M., and Weber, S.G. *Anal. Chem.* **1984,** *56,* 2560.

56. Bard, A.J., Crayston, J.A., Kittlesen, G.P., Shea, T.V., and Wrighton, M.S. *Anal. Chem.* **1986**, *58,* 2321.

57. Sreenivas, G., Ang, S.S., Fritsch, I., Brown, D.J., Gerhardt, G.A., and Woodward, D.J. *Anal. Chem.* **1996,** *68,* 1858.

58. Beilby, A.L., and Carlsson, A. *J. Electroanal. Chem.* **1988,** *248*, 283.

59. Tabei, H., Takahashi, M., Hoshino, S., Niwa, O. and Horiuchi, T. *Anal. Chem.* **1994,** *66,* 3500.

60. Kaplan, M.L., Scmidt, P.H., Chen, C.H., and Walsh, Jr., W.M. *Appl. Phys. Lett.* **1980,** *36(10),* 867.

61. Fan, Z.H., and Harrison, D.J. *Anal. Chem.* **1994,** *66,* 177.

62. Maloy, J.T. *Laboratory Techniques in Electroanalytical Chemistry.* 2nd ed., Marcel Dekker, Inc. New York, **1996**.

63. Schroeder, T. J., Jankowski, J.A., Kawagoe, K.T., Wightman, R. M., Lefrou, C. and Amatore, C. *Anal. Chem.* **1992,** *64,* 3077.

64. Licht, S., Cammarata, V., and Wrighton, M.S. *Science.* **1989,** *243,* 1176.

65. Lesczyszyn, D.J., Jankowski, J.A., Viveros, O.H., Diliberto, E.J., Near, J.A., and Wightman, R.M. *J. Biol. Chem.* **1990,** *265,* 14736.

66. Wightman, R.M., Jankowski, J.A., Kennedy, R.T., Kawagoe, K.T., Schroeder, T.J., Leszczyszyn, D.J., Near, J.A., Diliberto, E.J., and Viveros, O.H. *Proc. Natl. Acad. Sci.* **1991,** *88,* 10754.

67. Huang, L., Shen, H., Atkinson, M.A., and Kennedy, R.T. *Proc. Natl. Acad. Sci.* **1995,** *92,* 9608.

68. Kennedy, R.T., Huang, L., Atkinson, M.A., Dush, P. *Anal. Chem.* **1993,** *65,* 1882.

69. Kennedy, R.T., Huang, L., and Aspinwall, C.A. *J. Am. Chem. Soc.* **1996,** *118,* 1795.

70. Aspinwall, C.A., Brooks, S.A., Huang, L., Lakey, J.R.T., Kennedy, R.T., submitted for publication, **1997.**

71. Orci, L. *Diabetes.* **1982**, *31,* 538.

APPENDIX A
SWITCHING CIRCUIT SCHEMATIC

The following diagram is a schematic for the Ensman EI-401 dual integrator headstage switching system.

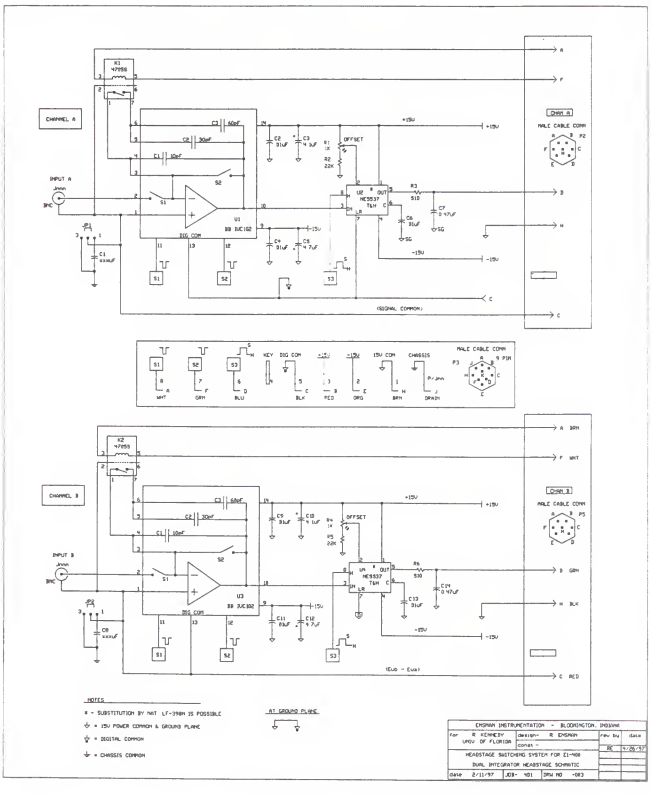
CHANNEL A
INPUT A
BNC
U1
BB INC102
U2
HC9537
TLH
OFFSET
+15V
-15V
DIG COM
(SIGNAL COMMON)
CHAN A
MALE CABLE CONN
P2
P3
S1
S2
S3
KEY
DIG COM
+5V
15V COM
CHASSIS
MALE CABLE CONN
9 PIN
CHANNEL B
INPUT B
U3
BB INC102
CHAN B
(GND - Case)
NOTES
* = SUBSTITUTION BY MAT LF-398N IS POSSIBLE
= 15V POWER COMMON & GROUND PLANE
= DIGITAL COMMON
= CHASSIS COMMON
AT GROUND PLANE
EMSMAN INSTRUMENTATION - BLOCKNOTION, INSIMM
For: R KENNEDY
UNIV OF FLORIDA
Design: R EMSMAN
Comm:
HEADSTAGE SWITCHING SYSTEM FOR EI-400
DUAL INTEGRATOR HEADSTAGE SCHMATIC
Date: 2/11/97
JOB: 401
DRW NO: -003
Rev by
date
RK
1/25/97

APPENDIX B
PARALLEL OPPOSED RECYCLING DETECTION SIMULATION PROGRAM

The following is an example of a recycling detector simulation program. The source code was written in QuickBASIC version 4.5

```
'Filename is Recycl6c.bas
'This program does multiple simulations for the same parameters and
'Gives an average result for each and the overall average
'This program will do 2-d random walks for a specified # of molec.
'And keep track of # of cycles a molecule makes between two trodes and distribution of
'These #'s
'Can change distance of trodes
'Starts all particles in the center between the two trodes
'Trodes can be different width than channel

'$DYNAMIC
DECLARE SUB BACKUP ()
DECLARE FUNCTION randnum ()
COMMON SHARED DIREC
COMMON SHARED LE

SCREEN 12
RANDOMIZE TIMER

CLS

PRINT "This program simulates behavior of electroactive molecules between two
parallel"
PRINT "opposed electrodes, one at an oxidizing potential, one at a reducing potential.";
PRINT "a specified number of simulations are done with the same parameters."
PRINT "the average # of times each molecule is recycled (reduced more than once)"
PRINT "is calculated for each simulation."
PRINT
DO

CLEAR
```

```
INPUT "How many molecules do you want to analyze "; NM&
INPUT "How wide should the detection electrode be (um)"; DTROD
INPUT "How wide should the recycling electrode be (um)"; RTROD
INPUT "How far apart should the electrodes be (depth of channel) (um)"; DIS
INPUT "How wide should the channel be (opposite walls) (um)"; WID
INPUT "What is the length of the channel (mm)"; LENG
INPUT "What should the step size be (UM)"; LE
INPUT "What is the volumetric flow rate into detector (nl/min)"; FLOW
INPUT "How many simulations would you like to do with these parameters"; SIM
INPUT "What name would you like the results stored under"; FILENAME$

DIM SHARED P(NM&)
DIM SHARED OXID(SIM)
DIM SHARED EFFIC(SIM)
DIM SHARED RECYCLED(SIM)
DIM SHARED AVE(1 TO SIM)    'Varible to keep track ofaverages of simulations
DIM SHARED I(NM&) AS SINGLE
DIM SHARED J(NM&) AS SINGLE

VOL = ((WID / 10000) * (DIS / 10000) * (LENG / 10)) * 1000 * 1000  'Volume in nL
AREA = (LENG / 10) * (DTROD * .0001)
RAREA = (LENG / 10) * (RTROD * .0001) 'Recycling trode area


PRINT "The area of the detection trode is"; AREA; "cm squared and "
PRINT "the volume of the detector cell is"; VOL; "nl."

Time = (VOL / FLOW) * 60
TS = ((LE * .0001) ^ 2) / (2 * .000006)    'Calc time per step from Einstein equation
LW& = Time / TS                    'Calc # of steps

MAX& = (LE * LW&) / (2 * DIS)
'Gives # for estimate of maximum times analyte can be recycled-LE is length of step


RIGHT = WID / 2              'Spaces trodes on either side of center point
LEFT = -(WID / 2)
TOP = DIS / 2
BOTTOM = -(DIS / 2)
TOTAL = 0

OPEN FILENAME$ FOR OUTPUT AS #1
WRITE #1, SIM    'Number of simulations
WRITE #1, NM&    'Number of particles
WRITE #1, DTROD  'Width of detec trode
```

```
WRITE #1, RTROD  'Width of recycling trode
WRITE #1, LENG   'Length of channel
WRITE #1, DIS    'Distance between trodes (depth)
WRITE #1, WID    'Width of channel
WRITE #1, FLOW   'Flow rate
WRITE #1, AREA   'Detection trode area
WRITE #1, VOL    'Volume of detector
WRITE #1, Time   'Residence time
WRITE #1, TS     'Time per step


FOR HH = 1 TO SIM     'Loop to start each simulation

H = 0                 'Keeps track of recycles
m = 0                 'Keeps track of initial detections

FOR Z = 1 TO NM&      'Calculates starting position (here 0,0) for each particle
P(Z) = 11             '11 indicates initial state of analyte (reduced)
I(Z) = 0              'Initial x position
J(Z) = 0              'Initial y  Position
NEXT Z

FOR n = 1 TO LW&      'Loop to start each step of walk
  FOR L = 1 TO NM&    'Indicates which particle
X = randnum           'Calls random number
Y = randnum

I(L) = I(L) + X
J(L) = J(L) + Y

IF I(L) >= RIGHT THEN I(L) = RIGHT    'Reflects particle when it hits trode
IF I(L) <= LEFT THEN I(L) = LEFT      'Sets up boundries for particles
IF J(L) <= BOTTOM THEN J(L) = BOTTOM
IF J(L) >= TOP THEN J(L) = TOP

            'Have selected top as the reducing trode
            'Bottom is oxidation or detection trode

IF J(L) = BOTTOM AND I(L) >= (-DTROD / 2) AND I(L) <= (DTROD / 2) AND P(L)
= 11 THEN
     P(L) = 12
     m = m + 1
            'Keeps track of # of particles initially detec. for conv. effic.
            'For initial oxidation of analyte
```

```
ELSEIF J(L) = TOP AND I(L) >= (-RTROD / 2) AND I(L) <= (RTROD / 2) AND P(L)
= 12 THEN
    P(L) = 14
        'this variable indicates REDUCTION    P(L) = 14)

ELSEIF J(L) = BOTTOM AND I(L) >= (-DTROD / 2) AND I(L) <= (DTROD / 2) AND
P(L) = 14 THEN
   P(L) = 12   'Indicates oxidation
   H = H + 1    'Keeps track of how many times
        'Hits wall in reduced state to be
        'Recycled-counts # of cycles
END IF
NEXT L

LOCATE 20, 10: PRINT "Time (s):"; (TS * n)

NEXT n          'Starts next step of walk
OXID(HH) = m    '# of particles oxidized at least one time
EFFIC(HH) = m / NM&  'Conversion efficiency for this sim
RECYCLED(HH) = H     '# of recycles for this sim (for all particles ADDED UP)
AVE(HH) = H / NM&    'ave # of recycles per particle
PRINT
PRINT "Done with simulation #"; HH
NEXT HH

CLS
PRINT "Detection electrode width:"; DTROD; "um area:"; AREA; "cm squared"
PRINT "Recycling electrode width:"; RTROD; "um"
PRINT "Channel  width: "; WID; "um, Length:"; LENG; "mm, Depth:"; DIS; "um"
PRINT "Detector volume:"; VOL; "nl.  Flow rate:"; Flow; "nL/Min"
PRINT NM&; "Molecules each traveled"; LW&; "Steps in";
PRINT " a time of"; Time; "sec."
PRINT "FILENAME:"; FILENAME$
PRINT : PRINT "# of simulation", "ave. # of cycles"
TOTALR = 0
FOR UU = 1 TO SIM
PRINT UU, , AVE(UU)
WRITE #1, AVE(UU), EFFIC(UU)
TOTALR = TOTALR + AVE(UU)
TOTALE = TOTALE + EFFIC(UU)
NEXT UU

EAVE = TOTALE / SIM
OAVE = TOTALR / SIM
```

```
FOR KK = 1 TO SIM
DSQUAREDE = (EFFIC(KK) - EAVE) ^ 2
DSQUARED = (AVE(KK) - OAVE) ^ 2
SUMDSQUARED = SUMDSQUARED + DSQUARED
SUMDSQE = SUMDSQE + DSQUAREDE
NEXT KK
STDDEV = SQR(SUMDSQUARED / SIM)
STDDEVE = SQR(SUMSQE / SIM)

PRINT : PRINT "Average # of cycles for"; SIM; "simulations:"; OAVE; "+/-"; STDDEV
PRINT "Average conversion effic.:"; EAVE; "+/-"; STDDEVE
PRINT
PRINT #1, "Ave. cycles", "Ave conv. effic"
WRITE #1, OAVE, "+/-", STDDEV, EAVE, "+/-", STDDEVE
CLOSE #1
INPUT "Would you like to do a different simulation (Y/N)"; QUES$
IF QUES$ = "Y" OR QUES$ = "y" THEN CLS
LOOP WHILE QUES$ = "Y" OR QUES$ = "y" OR QUES$ = "YES" OR QUES$ =
"yes"

REM $STATIC
FUNCTION randnum
DIREC = RND
IF DIREC > .5 THEN
    randnum = LE
ELSEIF DIREC > 0 THEN
    randnum = -LE
END IF
                                    END FUNCTION
```

APPENDIX C
CELL EXOCYTOSIS SIMULATION PROGRAM

The following is an example of a program written for simulation of exocytosis product diffusion and detection at a microelectrode. The source code was written in QuickBASIC version 4.5.

```
'Program name 3DCELL1E.BAS
'Three Dimensional Random Walk-Prog 1
DECLARE FUNCTION WALK.JUMP% ()
DECLARE SUB PROGRAM.BEGINNING ()
DECLARE SUB PROGRAM.SCREEN ()

'Random walk program---3 dimensional
'The X,Y, and Z movements must be independent
'Calculates ellipsoidal shaped trode polished at 30 degrees
'$DYNAMIC
COMMON SHARED AVERAD AS SINGLE
COMMON SHARED LAXIS AS SINGLE
COMMON SHARED LAXIS2 AS SINGLE
COMMON SHARED AVEAXIS AS SINGLE
COMMON SHARED DIFFCOEF AS SINGLE    'Diffusion coefficient
COMMON SHARED NUMPART AS LONG    'Number of particles for each simulation
COMMON SHARED RESOLUTION AS LONG  'The inverse of the step size in microns
COMMON SHARED SIMUL AS LONG      'Number of simulations to do
COMMON SHARED ELECRAD AS LONG    'Electrode radius
COMMON SHARED ELECDIST AS LONG   'Distance between the cell and the trode
COMMON SHARED CELLRAD AS LONG    'Cell radius
COMMON SHARED INSULWIDTH AS LONG  'Thickness of insulator around trode
COMMON SHARED FILENAME AS STRING    'The filename to be written
COMMON SHARED KIN.FACTOR AS SINGLE  'Kinetic factor
COMMON SHARED DIST.DOWN AS LONG   'Vertical spacing from pole of cell

DO     'Do loop to put the program into batch mode to perform 10 simulations with
       'specified particles per simulation

CALL PROGRAM.BEGINNING     'Subprogram to get input parameters
```

```
SEC$ = MID$(TIME$, 7, 2)          'Gets # of seconds from clock
            'Gets from end of hh:mm:ss
                                  'This is given as a string value
SEED = VAL(SEC$)                  'Converts string to numeric value
                                  'Pick a random number to reseed generator
RANDOMIZE (SEED)                  'Uses second value to reinitialize
                                  'Random number generato r

SIZE = NUMPART                    'Indicates # of molecules to do
                                  'Use input statement for this
REDIM X(SIZE) AS SINGLE           'X coordinate
REDIM Y(SIZE) AS LONG             'Y coordinate 'if cell radii big need to make long
                                  'Integer--overflows when calc start position
REDIM Z(SIZE) AS LONG             'Z coordinate
REDIM ITERAT(SIZE) AS LONG        'Track when the particle may be oxidized
REDIM OXNUM(SIZE) AS LONG         'Number of times a particle is oxidized

FOR K = 1 TO SIMUL STEP 1         'Runs 10 simulations-can put as variable
    CALL PROGRAM.SCREEN           'Screen which is displayed during simulation
    LOCATE 4, 55: PRINT FILENAME
    LOCATE 5, 55: PRINT USING "##.##"; 1 / RESOLUTION
    LOCATE 6, 55: PRINT USING "##.##"; ELECRAD / RESOLUTION
    LOCATE 7, 55: PRINT USING "##.##"; INSULWIDTH / RESOLUTION
    LOCATE 8, 55: PRINT USING "##.##"; (ELECDIST - CELLRAD) /
RESOLUTION
    LOCATE 9, 54: PRINT USING "###.##"; CELLRAD / RESOLUTION
    LOCATE 10, 54: PRINT USING "#.######"; DIFFCOEF
    LOCATE 12, 38: PRINT USING "##"; K
    LOCATE 12, 44: PRINT USING "##"; SIMUL
    LOCATE 15, 11: PRINT USING "  ####    ##.####^^^^  ######    ######
#### "; 0; 0; SIZE; 0; 0

SELECT CASE K
                  'Select which of the 10 is running
    CASE 1
        OPEN FILENAME + ".DT0" FOR OUTPUT AS #3   'EXTENSION FOR
SIMULATION NUMBER
    CASE 2
      OPEN FILENAME + ".DT1" FOR OUTPUT AS #3
   CASE 3
      OPEN FILENAME + ".DT2" FOR OUTPUT AS #3
    CASE 4
      OPEN FILENAME + ".DT3" FOR OUTPUT AS #3
    CASE 5
      OPEN FILENAME + ".DT4" FOR OUTPUT AS #3
```

```
        CASE 6
         OPEN FILENAME + ".DT5" FOR OUTPUT AS #3
        CASE 7
         OPEN FILENAME + ".DT6" FOR OUTPUT AS #3
       CASE 8
         OPEN FILENAME + ".DT7" FOR OUTPUT AS #3
        CASE 9
         OPEN FILENAME + ".DT8" FOR OUTPUT AS #3
       CASE 10
         OPEN FILENAME + ".DT9" FOR OUTPUT AS #3
        CASE ELSE
END SELECT
WRITE #3, 1 / RESOLUTION      'STEP SIZE
WRITE #3, ELECRAD / RESOLUTION   'ELECTRODE RADIUS
WRITE #3, INSULWIDTH / RESOLUTION    'INSULATION THICKNESS
WRITE #3, (ELECDIST - CELLRAD) / RESOLUTION     'ELECTRODE DISTANCE
WRITE #3, CELLRAD / RESOLUTION 'CELL RADIUS
WRITE #3, DIFFCOEF
WRITE #3, DIST.DOWN / RESOLUTION' OFF AXIS VERTICAL POSITION
WRITE #3, KIN.FACTOR
WRITE #3, NUMPART
LAXIS = ((ELECRAD / RESOLUTION) * 2) / .819152      'SIN 90* just entered as 1
                                                    'SIN 55 Deg = .819152
                                'Above-calc length (diameter) of ellipse (long axis)
LRADIUS = LAXIS / 2
LRADIUSN = LRADIUS * RESOLUTION  'Gives radius normalized
AVERAD = CINT((LRADIUSN + ELECRAD) / 2)
SIZE = NUMPART                          ' SIN 60 deg as radians
FOR I = 1 TO SIZE                       'Calc start position for each molec
    Z(I) = 0
    Y(I) = CELLRAD - DIST.DOWN
    IF DIST.DOWN = 0 THEN
        X(I) = 0
    ELSE
       X(I) = SQR(CELLRAD * CELLRAD - Y(I) * Y(I)) 'Calc off axis position
    END IF
    ITERAT(I) = 1          'Sets all particles to reduced form initally
    OXNUM(I) = 0           'No particle oxidized intitially
NEXT I
OPEN FILENAME + ".TAT" FOR OUTPUT AS #4
PRINT #4, USING "Step size 'Resolution'(uM): ##.##"; 1 / RESOLUTION
PRINT #4, USING "Electrode Radius (uM):  ##.##"; ELECRAD / RESOLUTION
PRINT #4, USING "Insulation thickness (uM):  ##.##"; INSULWIDTH / RESOLUTION
PRINT #4, USING "Electrode Distance (uM):  ##.##"; (ELECDIST - CELLRAD) /
RESOLUTION
```

```
PRINT #4, USING "Cell Radius (uM): ##.##"; CELLRAD / RESOLUTION
PRINT #4, USING "Diffusion Coefficient (cm^2/s): #.######"; DIFFCOEF
PRINT #4, USING "Kinetic Factor Used: ##.####^^^^"; KIN.FACTOR
PRINT #4, USING "Release Point (x-y-z):  (##.####-##-##)"; X(1) / RESOLUTION;
Y(1) / RESOLUTION; Z1 / RESOLUTION
CLOSE #4
LOCATE 11, 50: PRINT USING "(##.####-##-##)"; X(1) / RESOLUTION; Y(1) /
RESOLUTION; Z1 / RESOLUTION

TIME = (.0001 / RESOLUTION) * (.0001 / RESOLUTION) / (2 * DIFFCOEF)

LOOPS = 0                          'Time per increment
DEAD = 0
DEADINST = 0
DO
    LOOPS = LOOPS + 1
        FOR I = 1 TO SIZE STEP 1       'For each particle
            XSTEP = WALK.JUMP          'Jump +1 or -1 in each
            YSTEP = WALK.JUMP          'of the three directions
            ZSTEP = WALK.JUMP
            X(I) = X(I) + XSTEP
            Y(I) = Y(I) + YSTEP
            Z(I) = Z(I) + ZSTEP
            IF X(I) * X(I) + Y(I) * Y(I) + Z(I) * Z(I) < CELLRAD ^ 2 THEN
              X(I) = X(I) - XSTEP
              Y(I) = Y(I) - YSTEP    'Will reflect if hits cell
              Z(I) = Z(I) - ZSTEP
            END IF
            IF Y(I) < 0 THEN
              X(I) = X(I) - XSTEP
              Y(I) = Y(I) - YSTEP    'Will reflect if hits bottom
              Z(I) = Z(I) - ZSTEP
            END IF
            IF Y(I) > ELECDIST THEN
              IF (X(I) * X(I) + Z(I) * Z(I)) < (AVERAD + INSULWIDTH) ^ 2
THEN
                X(I) = X(I) - XSTEP
                Y(I) = Y(I) - YSTEP    'Will reflect if hits
                Z(I) = Z(I) - ZSTEP    'Insulation on side
              END IF
        END IF
            IF Y(I) = ELECDIST THEN    'When particle hits trode
              'This prog. sets x as long axis-could be different
              SELECT CASE ((X(I) ^ 2) + (Z(I) ^ 2))
                CASE IS <= AVERAD * AVERAD
```

```
                    X(I) = X(I)
                    Y(I) = Y(I)
                    Z(I) = Z(I)
                    IF LOOPS > ITERAT(I) AND OXNUM(I) < 1 THEN
                      DEAD = DEAD + 1
                      DEADINST = DEADINST + 1
                      IF KIN.FACTOR = 0 THEN
                        NEWIT = 3000
                      ELSE
                        NEWIT = (LOG(RND) / (-1 * KIN.FACTOR * TIME))
                      END IF
                      IF NEWIT <= 3000 THEN       'Set time to cyclization
                        ITERAT(I) = LOOPS + CINT(NEWIT)
                      ELSE
                        ITERAT(I) = 4000
                      END IF
                      OXNUM(I) = OXNUM(I) + 1
                    ELSE              'Particle is left alone
                    END IF
                   CASE IS < (AVERAD + INSULWIDTH) * (AVERAD +
INSULWIDTH)
                      X(I) = X(I) - XSTEP
                      Y(I) = Y(I) - YSTEP   'Will reflect if hits insulation
                      Z(I) = Z(I) - ZSTEP
                   CASE ELSE
                 END SELECT
               END IF
             NEXT I
         WRITE #3, DEADINST
         LOCATE 15, 11: PRINT USING " ####   ##.####^^^^  ######   ######
#### "; LOOPS; LOOPS * TIME; SIZE - DEAD; DEAD; DEADINST
       DEADINST = 0
        LOOP UNTIL LOOPS > 2999 OR DEAD > 9999
        CLOSE #3
      COLOR 3, 0
NEXT K
LOCATE 20, 5: PRINT "FINALLY FINISHED! Would you like to rerun the program ?:"
LOCATE 20, 65: INPUT "", RESPONSE$
LOOP WHILE UCASE$(RESPONSE$) = "Y"
END

REM $STATIC
SUB PROGRAM.BEGINNING
CLS
COLOR 3, 0
```

```
LOCATE 1, 25: PRINT "THREE DIMENSIONAL RANDOM WALK"
FOR COUNT = 1 TO 29 STEP 1              'Loop draws double line
    LOCATE 2, 24 + COUNT: PRINT CHR$(205)
NEXT COUNT

LOCATE 6, 5: INPUT "Enter the step size 'resolution' (um) ", ANSWER
RESOLUTION = CINT(1 / ANSWER)
LOCATE 7, 5: INPUT "Enter the electrode radius (um): ", ANSWER
ELECRAD = CINT(RESOLUTION * ANSWER)
LOCATE 8, 5: : INPUT "Enter the thickness of the insulator (um):", ANSWER
INSULWIDTH = CINT(RESOLUTION * ANSWER)
LOCATE 9, 5: INPUT "Enter the cell radius (um): ", ANSWER
CELLRAD = CINT(RESOLUTION * ANSWER)
LOCATE 10, 5: INPUT "Enter the distance between the cell and the electrode (um):",
ANSWER
ELECDIST = CINT(RESOLUTION * ANSWER) + CELLRAD
LOCATE 11, 5: INPUT "Enter the base file name: ", FILENAME
LOCATE 12, 5: INPUT "Enter vertical distance from pole (um): ", ANSWER
DIST.DOWN = RESOLUTION * ANSWER
LOCATE 13, 5: INPUT "Enter the kinetic factor: ", KIN.FACTOR
LOCATE 14, 5: INPUT "How many simulations with these parameters ", SIMUL
LOCATE 15, 5: INPUT "How many particles for each simulation ", NUMPART
LOCATE 16, 5: INPUT "What is the diffusion coefficient (cm^2/s)", DIFFCOEF
END SUB

SUB PROGRAM.SCREEN
CLS
LOCATE 3, 10: PRINT CHR$(218)
LOCATE 3, 71: PRINT CHR$(191)
LOCATE 13, 10: PRINT CHR$(192)
LOCATE 13, 71: PRINT CHR$(217)
FOR K = 11 TO 70 STEP 1
    LOCATE 3, K: PRINT CHR$(196)
    LOCATE 13, K: PRINT CHR$(196)
NEXT K
FOR K = 4 TO 12 STEP 1
    LOCATE K, 10: PRINT CHR$(179)
    LOCATE K, 71: PRINT CHR$(179)
NEXT K
LOCATE 4, 21: PRINT "Base file name being processed:"
LOCATE 5, 21: PRINT "Step size 'resolution'(um): "
LOCATE 6, 21: PRINT "ELECTRODE RADIUS (um):"
LOCATE 7, 21: PRINT "Insulation thickness (um):"
LOCATE 8, 21: PRINT "Electrode distance (um):"
LOCATE 9, 21: PRINT "Cell radius (um):"
```

```
LOCATE 10, 21: PRINT "Diffusion coeffiecent (cm^2/s) "
LOCATE 11, 21: PRINT "Release point (x-y-z):"
LOCATE 12, 21: PRINT "Processing case #  of  cases "
LOCATE 14, 12: PRINT "Iteration   Time   Remaining   Used  Derivative"
COLOR 14, 0
LOCATE 2, 30: PRINT "DO NOT TURN ME OFF!!!"
END SUB


FUNCTION WALK.JUMP%
TMP = RND
SELECT CASE TMP
    CASE IS > (1 / 2)      'STEP + 1
        WALK.JUMP = 1
    CASE IS > 0            'STEP -1
        WALK.JUMP = -1
    CASE ELSE
        WALK.JUMP = 0
END SELECT
END FUNCTION
```

BIOGRAPHICAL SKETCH

Sunday Ann Brooks was born October 26, 1969, in Indianapolis, Indiana. She earned a Bachelor of Science degree in chemistry from the University of Central Florida in April 1992. She then began graduate school in analytical chemistry at the University of Florida in August 1992. During graduate course work she developed interests in bioanalytical methods and separation science, and joined the research group of Dr. Robert T. Kennedy. She completed her research and obtained her Doctor of Philosophy degree in August of 1997.

I certify that I have read this study and that in my opinion it conforms to acceptable standards of scholarly presentation and is fully adequate, in scope and quality, as a dissertation for the degree of Doctor of Philosophy.

Robert T. Kennedy, Chair
Associate Professor of Chemistry

I certify that I have read this study and that in my opinion it conforms to acceptable standards of scholarly presentation and is fully adequate, in scope and quality, as a dissertation for the degree of Doctor of Philosophy.

Anna F. Brajter-Toth
Associate Professor of Chemistry

I certify that I have read this study and that in my opinion it conforms to acceptable standards of scholarly presentation and is fully adequate, in scope and quality, as a dissertation for the degree of Doctor of Philosophy.

James D. Winefordner
Graduate Research Professor of Chemistry

I certify that I have read this study and that in my opinion it conforms to acceptable standards of scholarly presentation and is fully adequate, in scope and quality, as a dissertation for the degree of Doctor of Philosophy.

William T. Weltner
Professor of Chemistry

I certify that I have read this study and that in my opinion it conforms to acceptable standards of scholarly presentation and is fully adequate, in scope and quality, as a dissertation for the degree of Doctor of Philosophy.

Thomas W. Vickroy
Associate Professor of Veterinary Medicine

This dissertatioin was submitted to the Graduate Faculty of the Department of Chemistry in the College of Liberal Arts and Sciences and was accepted as partial fulfillment of the requirements for the degree of Doctor of Philosophy.

August 1997

_____

Dean, Graduate School